The physical oceanography of Fortune Bay, an overview

Sebastien Donnet [a,d,*], Pascal Lazure [b], Andry Ratsimandresy [c], Guoqi Han [a]

[a] Fisheries and Oceans Canada, Institute of Ocean Sciences, 9860 West Saanich Road, Sidney, BC, V8L 4B2, Canada
[b] Ifremer, Laboratoire d'Océanographie Physique et Spatiale, Centre Bretagne, ZI de la Pointe du Diable, CS 10070, 29280 Plouzané, France
[c] Fisheries and Oceans Canada, Northwest Atlantic Fisheries Centre, 80 East White Hills Rd, St. John's NL, A1C 5X1, Canada
[d] Université de Brest Occidentale, Ecole Doctorale N°598 Science de la Mer et du littoral, Brest, France

ABSTRACT

This paper describes the physical oceanography of Fortune Bay, a broad, mid-latitude fjord located in Newfoundland (Canada). Fortune Bay is subject to a strong seasonal stratification (0–16 °C sea-surface temperature range with up to 1 °C/m vertical gradient) influenced by local freshwater runoff, wind forcing and shelf inputs. Sea-ice is seldom present in the bay and unlikely to be of importance on the seasonal stratification and mixing processes. Fortune Bay is warmer than its adjacent shelf both at the surface (by about 2 °C) and at intermediate depths (by about 1 °C from 50–150 m). While the former is likely due to local freshwater runoff stratification influence, the latter is probably related to the warm, deep water input occurring in winter below sill depth and subsequently mixed with the intermediate layer via the input of a colder water mass flowing in summer and which eventually reaches the bottom as well. Currents are dominated by the 'weather band' (2–20 d) and characterized by energetic pulses associated with downwelling and upwelling events. Mean circulation is rather weak and the seasonal pattern obtained here did not reveal either the presence of a distinct estuarine circulation nor a strong influence of the main coastal current. Tidal currents are weak also and no inertial signal was observed. Estimates of water exchange between the inner and outer part of the bay were calculated using several methods and led to residence times of the order of a few to several months for the upper layers and of the order of a year for the bottom layer with a probable strong seasonal variability (larger residence time in summer for the upper layers). The "baroclinic pumping" processes, which include the downwelling/upwelling events, appear to be important players but more work is needed to better understand their nature and actual contribution.

1. Introduction

Fortune Bay is a large fjord-like embayment about 130 km long and 15 to 25 km wide located on the south coast of Newfoundland, a large island of eastern Canada (Fig. 1).

The physical oceanography of Fortune Bay is not well known. Some of the first accounts of its characteristics can be found in the detailed aid to navigation compiled by Gillpatrick and Gibson (1884) which states that the "currents are irregular in this bay"; a description that went virtually unchanged until now in subsequent aid to navigation publications (see Canadian Hydrographic Survey, 2022 for the most recent available). To our knowledge, it was not until the 1980–90's and the efforts of researchers and students from the Memorial University of Newfoundland (MUN) that the first oceanographic investigations were performed in Fortune Bay as part of two Master theses (de Young, 1983; Richard, 1987) and subsequent papers (de Young and Hay, 1987; Hay and

de Young, 1989; White and Hay, 1994; Richard and Haedrich, 1991). de Young's thesis focussed on deep water exchange between Fortune Bay and the adjacent shelf channels of Saint-Pierre and Hermitage (Fig. 1) while Richard's thesis described and discussed Fortune Bay's lower trophic biology as well as mesopelagic fish communities in relation to its physical oceanography. The deep water exchange studies (de Young and Hay, 1987; Hay and de Young, 1989; White and Hay, 1994) showed that Fortune Bay is seasonally vented by two very different water masses below sill depth (i.e. below about 120 m): cold and relatively fresh water (<2 °C and 32–33 in salinity) from Labrador Current origin water in summer (Labrador Current Water — LCW); warm and salty water from Atlantic origin (>4 °C and about 34.5 in salinity) in winter (Modified Slope Water — MSW, McLellan, 1957; Lauzier and Trites, 1958). This seasonal venting is due to the regional seasonality in wind, forcing these deep and dense waters over the sills: southwesterly wind in summer upwelling LCW over the sill of Saint-Pierre; northerly winds in winter upwelling MSW over the sill of Miquelon. de Young and Hay (1987) showed that the cold deep water renewal was 3 dimensional in nature, the width of the fjord being large enough for the dense, bottom

* Corresponding author at: Fisheries and Oceans Canada, Institute of Ocean Sciences, 9860 West Saanich Road, Sidney, BC, V8L 4B2, Canada.
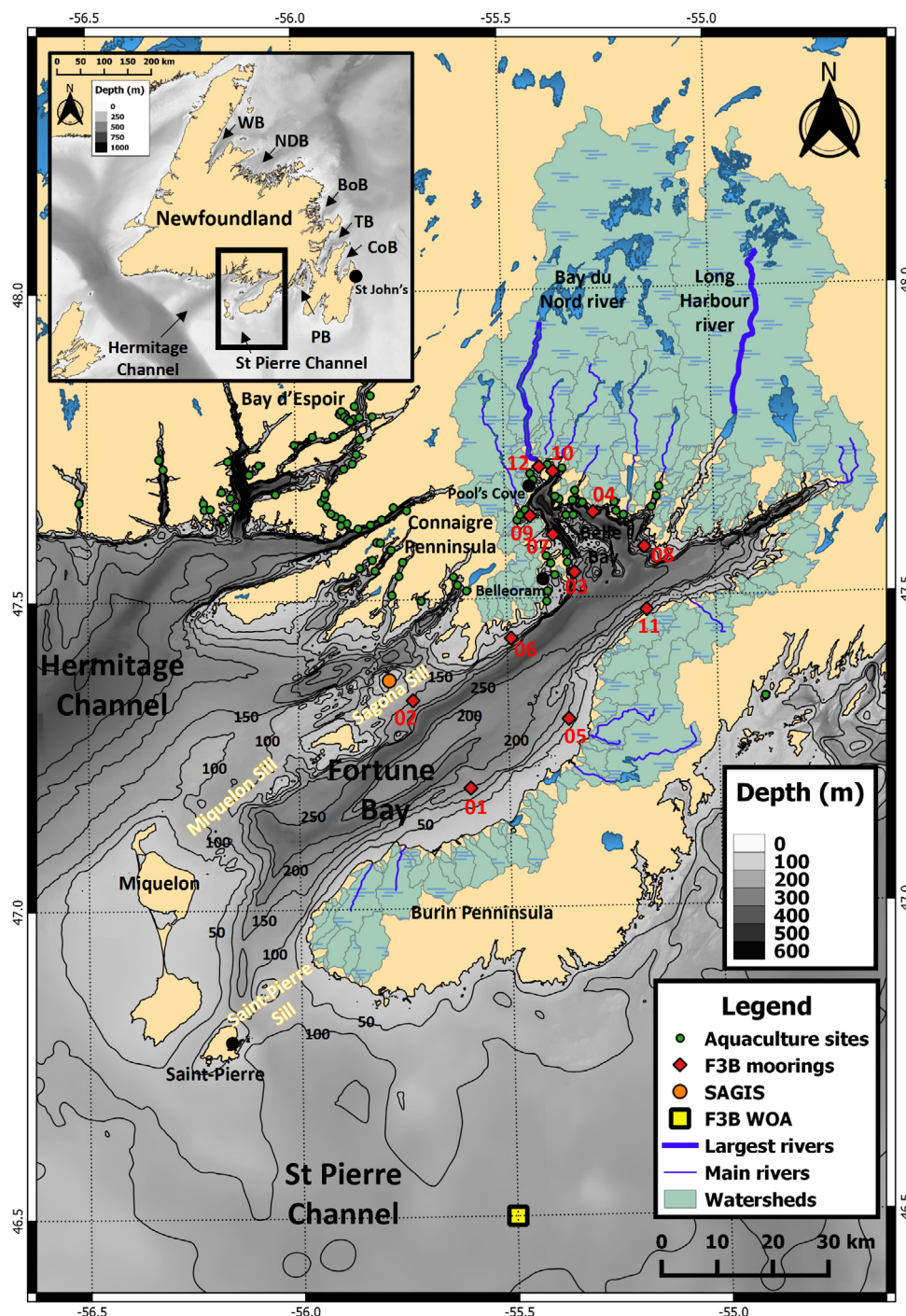E-mail address: sebastien.donnet@dfo-mpo.gc.ca (S. Donnet).

Fig. 1. Study area. Mooring sites from which ocean currents and water column temperature profiles were collected from 2015–17 are represented by red diamonds; the WOA temperature and salinity climatology data point is shown as a yellow square and the local, long-term, weather station is shown as an orange dot. Aquaculture sites (licences) are also represented, as green dots. Main bays surrounding the island of Newfoundland are indicated in the top-right corner insert (clockwise from the North: White Bay (WB), Notre Dame Bay (NDB), Bonavista Bay (BoB), Trinity Bay (TB), Conception Bay (CoB) and Placentia Bay (PB)).

flow to be affected by earth rotation. Hay and de Young (1989) described the seasonal processes of renewal and explained their forcing mechanisms while White and Hay (1994) showed that the cold water renewal flow is strongly modulated by the tide as well as by the interaction of the cold density current with bottom-trapped wave or interior basin modes at periods of 2–3 days.

With a rapid development of finfish aquaculture in Belle Bay (Fortune Bay's main head) and surrounding areas in the early 2000s, an ambitious oceanographic program was started in 2009 by the Department of Fisheries and Oceans (DFO) to provide with the necessary background to study aquaculture–environment interactions. Of particular interest were the water column stratification and currents, key aspects to consider in aquaculture related studies such as dissolved oxygen depletion and particles dispersion (e.g. viruses, parasites and organic waste). The program focussed primarily on the collection of CTD+DO (Conductivity, Temperature and Depth + Dissolved Oxygen) profiles, moored ADCP (Acoustic Doppler Current Profiler) timeseries and drifter experiments (see DFO, 2016 for a summary of the program and its

key results and Donnet et al., 2018b,a; Ratsimandresy et al., 2019, 2020 for more details). The Coast of Bays was found to consist of three main regions with distinct geographic characteristics: Bay d'Espoir, Connaigre Peninsula and Fortune Bay (Fig. 1). Topography and freshwater runoff were found to be key aspects of differentiation (e.g. narrow fjord vs. broad bay and large vs. small runoff) influencing water column stratification and hydrodynamics (i.e. currents). A strong regional atmospheric heating and cooling seasonal cycle stratifies the near-surface water, i.e. top 20 m, a process amplified by the regionally variable freshwater runoff. The annual amplitude in sea-surface temperature is about 7 °C, i.e. 14 °C range, with stronger stratification in Bay d'Espoir and lesser stratification in Connaigre Peninsula (Donnet et al., 2018b). Tidal ranges in the region are small, about 2 m large tides and 1.4 m mean tides. Combined with the great depth of the bays considered, they result in small tidal currents except in areas of significant constrictions (e.g. sills of Bay d'Espoir) and in large flushing times from this forcing alone (order of months, or more). Wind, on the other hand, was found to be a major contributor to the generation of the very variable ocean currents observed (Salcedo-Castro and Ratsimandresy, 2013).

Despite those significant efforts, knowledge remains limited and the understanding of Fortune Bay ocean physics and dynamics is very much incomplete. The water column stratification annual cycle, coastal circulation and surface water exchange (or flushing) in particular, are unknown. The dominant processes affecting the ocean currents, their periodicity (if any exist) and effect on water exchanges, within the bay itself and/or with the shelf, for instance, have not been determined despite their importance to the studies of aquaculture–environment interactions.

The main objective of this paper is to provide a comprehensive and descriptive overview of the physical oceanography of Fortune Bay with a particular focus on upper water stratification and ocean currents including an assessment of their main physical drivers. Estimates of dominant energy bands of ocean currents, in the frequency domain, and of water exchanges will also be given to complement present knowledge.

Some figures and tables, herein labelled with an "S" prefix, are provided as supplementary material with this manuscript. Data used for and obtained from this study are available at: https://doi.org/10.6084/m9.figshare.13526366 and https://doi.org/10.17882/62314.

2. Bathymetric features

Fortune Bay is deep, reaching about 430 m within its main SW-NE oriented basin and about 600 m within its SE-NW oriented head (Belle Bay); on average, the bay is about 160 m deep. Fortune Bay has the particularity, compared to the other major bays surrounding Newfoundland, of being quasi-enclosed due to the presence of the Saint-Pierre and Miquelon (SPM) archipelago at its west and southwest boundary and to a series of islands, shallows and sills along most of its west to northwest boundary (Fig. 1). The limiting depth of the sills are about 110 m (Saint-Pierre) and 125 m (Miquelon and Sagona) restricting deep water exchange with the shelf. Two main channels, more than 200 m deep, and a shallower bank form the topography of Fortune Bay's southern part while its northern part is made of one main channel leading to Belle Bay, its most prominent head, and to a narrow inlet forming its much smaller NE head (about 15 km long, 2.5 km wide and more than 400 m in its deepest). The main channel connecting Fortune Bay to Belle Bay runs along the northern side, it is about 500 m maximum depth and ends by a sill of 100 m limiting depth connecting it to a widening head. On the southern side, a very narrow and steep canyon (about 500 m wide and about 600 m maximum depth) is separated from Fortune Bay

by a sill about 210 m depth. Belle Bay's own head is made of a wide and deep basin (about 5 × 5 km for 600 m maximum depth) connected to the canyon via a partial and deep sill. Belle Bay's center consists of a shallow bank (<100 m) on which rise several shoals and a few islands. Numerous side bays are present in Belle Bay, typically formed by one or more basins and one or more shallower sills (see Donnet et al., 2018b for details).

3. Temperature and salinity structure

3.1. Data reduction

Temperature and salinity data were mined from the Department of Fisheries and Oceans (DFO) Bedford Institute of Oceanography (BIO, http://www.bio.gc.ca/science/data-donnees/base/data-donnees/climate-climat-en.php, see also Gregory (2004) and Northwest Atlantic Fisheries Center (NAFC) archives to make a monthly climatology. The data consists primarily of XBT (eXpendable BathyThermograph), CTD and bottle profiles collected over the years on the Newfoundland shelves from a variety of platforms and institutions. The dataset was completed using recent CTD profiles collected by NAFC's aquaculture section (Ratsimandresy et al., 2014; Donnet et al., 2018a).

All data available within a square defined from 46.2 to 48 °N and 57.5 to 54.5 °W were first extracted from the databases within the largest possible time-period (01-Jan-1900 to 31-Dec-2018). The dataset was subsequently reduced to the Fortune Bay area using a polygon (Figure S1). In total, 810 profiles from BIO, 1130 profiles from NAFC and 806 profiles from NAFC's aquaculture section databases were extracted. The data was combined daily and spatially using a radius of 500 m; resulting in a dataset of 1750 averaged casts sampled over 911 stations. The earliest cast occurred the 15th of October 1925 and latest cast the 2nd of June 2018. Most of the sampling occurred after 1950 with a first broad peak from the late 50s to early 80s and a second from the mid-90s onward (Figure S2), however, most of the data prior to the mid-90s consisted of temperature profiles only. An important sampling effort occurred in 1981 and the recent sampling effort led by NAFC's aquaculture section from 2009 to 2017 is noticeable also. The dataset was split into two sub-polygons (areas): Fortune Bay (FB) and Belle Bay (BB), illustrated in Figure S1. The separation was based on the Region of Freshwater Influence (ROFI) estimated in Donnet et al. (2018b); that is, a region where the surface density field is likely dominated by freshwater inputs and thus where the surface water structure is likely to differ from the rest of the bay. The profiles were checked visually to remove dubious casts or spikes. Temperature and Salinity values at depth shallower than 1 m and salinity values below 20 were removed due to uncertainty in the data. Practical Salinity values (as provided in the databases) were converted to Absolute Salinity values using TEOS-10 relationships (IOC, SCOR, IAPSO, 2010; McDougall and Barker, 2011) and assuming a δS_A equal to 0 (as advised in Pawlowicz, 2013 when working with coastal waters).

Monthly averages were calculated by first spatially averaging every daily cast of each month on a year by year basis and then averaging this monthly series to obtain a monthly climate for each area. Standard deviations were calculated from this latter average, thus representing a measure of interannual variability. Monthly climate profiles were finally smoothed using a 'bin-median' filter, i.e. the median over a bin of a set depth range. A bin size of 5–50 m was used, varying amongst months and with depth, to take seasonal and vertical as well as sampling variability into account. Sampling coverage, both temporal and spatial, varies widely amongst this monthly climatology as illustrated in Figure S2; best coverage was obtained during the spring (April to June) while July and the winter season (January to March) are much less sampled, particularly in salinity.
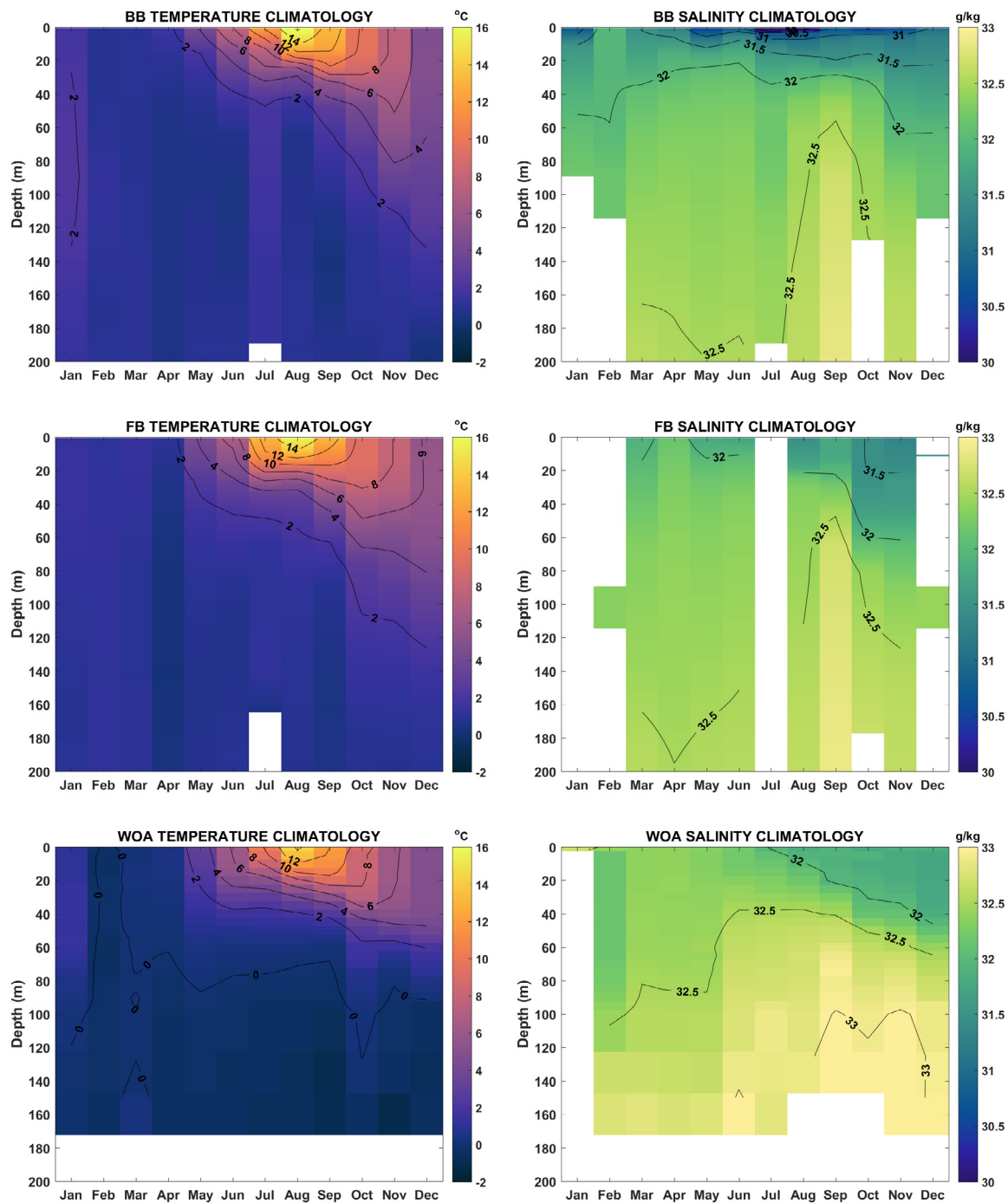
Fig. 2. Temperature and Salinity monthly climate of Belle Bay (BB), top, Fortune Bay (FB), middle, and shelf (WOA), bottom.

3.2. Monthly climate

Temperature and salinity climate of FB and BB are illustrated in Fig. 2. To compare the conditions of the bay with the shelf, monthly climatology data from the National Oceanic and Atmospheric Administration (NOAA) 1 degree gridded World Ocean Atlas (WOA18) were retrieved (https://www.nodc.noaa.gov/OC5/woa18/) and are also illustrated in Fig. 2. The closest 'upstream' data point with respect to the main coastal current of the region (i.e. the inner Labrador Current, see Loder et al., 1998 for a review) was used (see location in Fig. 1). To highlight the surface seasonal cycle, only the top 200 m are presented in Fig. 2.

The temperature climate results are consistent with the regional knowledge of the Newfoundland shelf (see Cyr et al., 2022 for the most recent update): a cold (<2 °C) near-homogeneous winter water column starts to stratify in early spring (April) and reaches a peak in August (about 15–16 °C near-surface, on average) before having its stratification breaking down in the fall and being completely mixed again by January. The temperature structure is similar in both BB and FB, though FB summer thermocline appears broader and BB near-surface temperature is slightly higher during the summer peak (August; by about 0.5 °C). Both areas are, more noticeably, warmer than the shelf in both the near surface (by about 2 °C in July) and at depth (by 1–2 °C below 50 m). Interannual variability, expressed as standard deviations,

is on the order of 1 °C or less (below 100–150 m, in particular) but can be as high as about 3.5 °C in late summer to early fall (August–September) in sub-surface (10–40 m).

The spatial contrast is more pronounced in salinity with the presence of a stronger surface halocline in BB from spring to fall (10–20 m depth). Near surface salinity in BB is less than 31 g/kg during these seasons (May–November); reaching a low of about 29.5 g/kg in July. In contrast, FB's near-surface salinity does not go below 31 g/kg and appears to be the lowest in October–November though we cannot tell what the situation is like during winter due to the lack of data for this season. Both regions, however, show a strong decrease in salinity at depth during the fall, illustrated by the deepening of the 32 g/kg isohaline (from about 40 m to more than 100 m). Interannual variability is smaller than 0.5 g/kg for the most part but can reach values up to 1 g/kg during summer months in BB (July–September). Overall, the variability is higher in BB than in FB within the upper 20 m (0.3 g/kg vs. 0.2 g/kg, annual average) while below that seasonal layer the variability is generally about 0.1 g/kg in both regions (annual average). Due to the scarcity of data, particularly for the months of January, February, July, October and December in FB, those estimates on interannual variability should be regarded as an order of magnitude. On the shelf outside the bay, the salinity structure is characterized by a seasonal freshening at the surface starting in summer, deepening in fall and most likely peaking in December (no data in January) with salinity within 31.5–32 g/kg range. Deeper, salinity appears to rise sharply in late spring (June) before stabilizing in summer and gradually decreasing in fall. These contrasting cycles (surface freshening vs. increasing salinity at depth) result in the making of the sharpest gradient in fall (October–December) around 50–60 m.

3.3. Deep water characteristics

Monthly Temperature–Salinity (T–S) regressions were made to better examine the seasonality of the water masses (details in supplementary material). This analysis shows the presence of a well-defined intermediate layer between the seasonally variable surface and bottom regions from June to September (characterized by a T–S slope of about −0.1 g/kg/°C). Warmer and saltier conditions are found from March to June and colder conditions were found from September to October below 120 m in both FB and BB (i.e. below outer sill depth). While reversals from warm to cold and from cold to warm occur in August and November in FB (respectively) it is not before September that the effects of cold water renewal are seen in BB's climatology and no clear reversal happen in November in this inner area of the fjord; indicating a time-lag of about a month in the change of deep water properties from FB to BB. Albeit limited by data coverage, these results are consistent with those presented by Hay and de Young (1989) who described influx of warm MSW from December to June and influx of cold LCW from May to December into Fortune Bay's main basin.

Using the most recent data collected (i.e. post 2010) and best covered months (i.e. May and November) it is possible to extend earlier investigations further and shed more light on spatial as well as interannual variability. It is also possible to illustrate potential changes in DO, this latter parameter being measured more systematically in recent years (see also Donnet et al., 2018a). Casts made in the deepest parts of Fortune Bay's outer basin (FB south) and Belle Bay's inner basin (BB north) were selected and are presented as T–S diagrams in Fig. 3 (A-D). The seasonal cycle is clear for both surface-intermediary waters (left from the black dots, representing sill depth) as well as deep waters (to the right from the black dots). The straightening of the T–S curves (A vs. B and C vs. D) indicates that mixing took place between the surface and sub-surface from May to November; probably both due to

surface forcing from the wind and sub-surface mixing due to LCW influx which initially occurs at intermediate depth before gradually eroding the bottom layer (Hay and de Young, 1989). This process(es) also tend to 'erase' the interannual variability (clearly visible in A&C but less so in B&D), particularly in the outer basin. At depth, the presence of MSW mixture, illustrated by a rising 'tail' below sill depth is evident in May in the outer basin (A). In the inner basin (C), the tail is much less pronounced and even show an opposite trend in some years, i.e. cooling with depth (years 2015&16). In November, this rising tail is still present (or newly re-formed) in the outer basin while being largely absent in the inner basin (B vs D). Overall, the outer basin waters are warmer than the inner basin waters below sill depth in May (by about 1 °C; see A vs. C) but can be slightly cooler in November by the presence of a more distinctive cold water 'knee' (B vs. D). The deepest part, however, show the presence of colder waters in the inner basin (indicated by a sharp dipping tail in D).

Both basins are fairly well oxygenated, with values of DO never below 8.5 mg/L and generally being well above 10 mg/L above sill depth in May (A&C). A seasonal cycle is also evident for this parameter, waters being more oxygenated in spring than in fall except, however and noticeably, in the deep part of the inner basin for some years (2015&16). Interestingly, these are associated with cooler water, even though the cold LCW, the likely origin of the cool temperatures, is much more oxygenated than the MSW (>10 mg/L vs. <6 mg/L, respectively; Donnet et al., 2018a). This may be an indication of longer stagnation/residence time in the inner basin. In general, and for both month presented, DO levels are higher in the outer basin than in the inner basin below sill depth (by about 1 mg/L; see A vs. C and B vs. D).

3.4. Stratification vs. rotation

By considering a surface layer thickness of 20 m (spring), 30 m (summer) and 80 m (fall) for the bay as a whole, density differences with the intermediate layer of 1 kg/m^3 (spring and fall in FB, and fall in BB), 2 kg/m^3 (spring in BB, summer in FB) and 4 kg/m^3 (summer in BB) and an average bay depth of 160 m, an internal Rossby radius range of 4–9 km is found. This range is smaller than the width of the bay (15–25 km) and implies an important effect of earth's rotation on Fortune Bay's water dynamics. Note that for the purpose of calculating this simple scaling parameter, we took a surface layer thickness corresponding to the bottom of the continuously stratified surface layer which occurs from spring to late fall. Those values are either smaller than (spring and fall) or larger than (summer) the limits found with the regression analysis using the 'inflection points' shown in Table S1 and Table S2.

4. Sea surface temperature, freshwater inputs and sea ice

Sea Surface Temperature (SST) is a useful observation to identify frontal areas (e.g. Cyr and Larouche, 2015), areas of significant mixing (e.g. Bisagni et al., 2001) and potential advection processes (e.g. Verbrugge and Reverdin, 2003). As it has been routinely and globally measured since the early 1980s from satellites, it is also a useful parameter to assess seasonal variations and long-term trends.

SST of the region were extracted from the National Oceanic and Atmospheric Administration (NOAA) Advanced Very High Resolution Radiometer (AVHRR) Pathfinder 5.3 reanalysis (Saha et al., 2018). Pathfinder 5.3 horizontal resolution is 4 km and its temporal resolution is daily from 25 August 1981 to present (see Casey et al., 2010 for a more complete description). Previous Pathfinder data compared favourably with in-situ data in the region (Galbraith and Larouche, 2013 and references therein) and
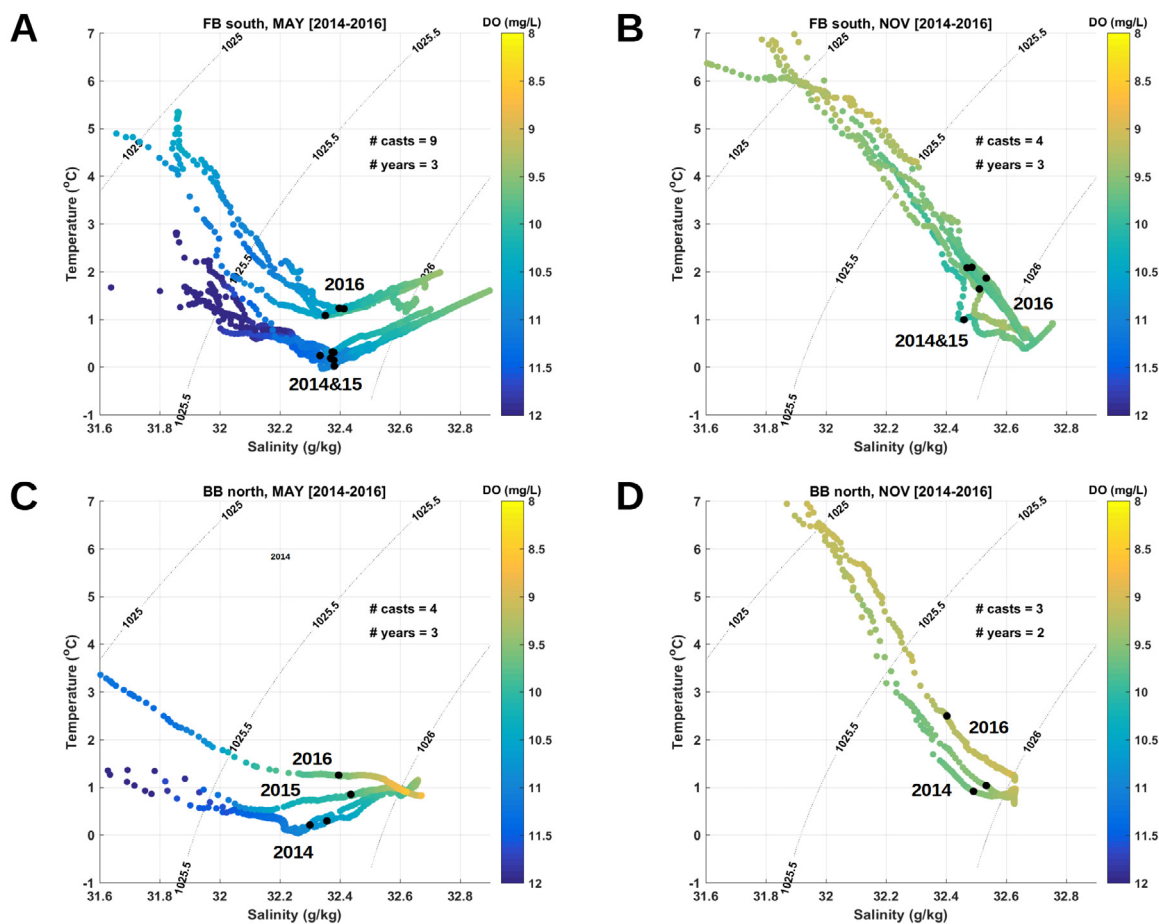
Fig. 3. T–S diagrams of Fortune Bay inner basin (FB south; C&D) and Belle Bay inner basin (BB north; E&F). TEOS-10 conservative temperature and absolute salinity are used. Water density is indicated by dotted lines (0 m reference level). Dissolved Oxygen (DO) values are represented in colour and the black dots indicate outer sill depth (120 m). Depth decrease (increase) to the left (right) of those dots. Number of casts used and years of observation are indicated on the figures as well as the years of the profiles. Note that most of the surface waters of BB (S<31.6) are not represented.

a more recent comparison using this version also showed good agreement with the most extensive in-situ data available of the region (Poitevin et al., 2022); providing some comfort to its use here. Data were first extracted for the time period covering 25 August 1981 to 31 December 2018 and for a region defined by an area 46.5 to 48 °N and 57.5 to 54.5 °W. To reduce potential land contamination, a buffer of 2 km, i.e. half a pixel size, was used along the NRCan high resolution coastline (see Donnet et al., 2018b for details of this later dataset).

Monthly average series were made from spatially averaging the daily series within a polygon of Fortune Bay, i.e. covering the whole bay. A total of 138 pixels were selected within the polygon (Figure S8). The monthly series obtained were then averaged per calendar month to get a monthly climate (Figure S9). Standard deviation was calculated from this latter average, representing a measure of interannual variability. Minimum and maximum of each averaged month of the monthly series were retained; representing coldest and warmest months observed within the period analysed (1985–2018). Data coverage is uneven both spatially and temporally, being substantially lower in Fortune Bay than in the domain covered in Fig. 4 (by about a factor 2, on average; Figure S10). On average, the coverage does not exceed 10% at any given point in Fortune Bay and is lower in from November to February (<5% on average) and the highest in August (∼8%). Maximums, representing the value at one single pixel, range between 4% (in December) to 16% (in September). Interestingly, a 'dip' appears in June–July (∼5% coverage, on average), most likely reflecting the

heavy fog conditions often experienced in this region during this period of the year (Canadian Hydrographic Survey (CHS), 2021).

To compare the SST annual cycle with Air Temperature (AT), local observations measured at Environment and Climate Change Canada (ECCC) Sagona Island (SAGIS) weather station (see Fig. 1 for location) were extracted to make a monthly climatology. The climatology (Figure S9) was created similarly to that of the SST for a slightly smaller period of available data (1994–2018). SST and AT are closely linked seasonally, peaking and lowering at the same time (August and February, respectively) although the coldest period lasts longer for the SST (February–March). August air and sea mean values are very close in August, 15.9 °C vs. 15.3 °C, respectively, but the sea is substantially warmer in February by more than 3 °C (−3.3 °C vs. 0 °C). Mean AT range is thus much larger at about 19.2 °C vs. 15.5 °C for the SST. Standard deviations were similar for both series and of the order of 1 °C although for the SST, it varies seasonally from a low of 0.7 °C in March to a high of 1.4 °C in July.

To get an idea of potential spatial variability in SST over the area of interest, seasonal maps were also created using data from the original extraction area. Straight monthly means were then calculated from the daily series at each available data point. Maps representative of the four seasons are presented in Fig. 4; to highlight spatial differences, the colour ranges of each map were adjusted to a mean ±1 std (standard deviation) range. Spatially, the most striking feature is the apparent propagation of a 'pulse' of cooler water propagating westward from winter to fall and a persistent cold water area along the eastern and
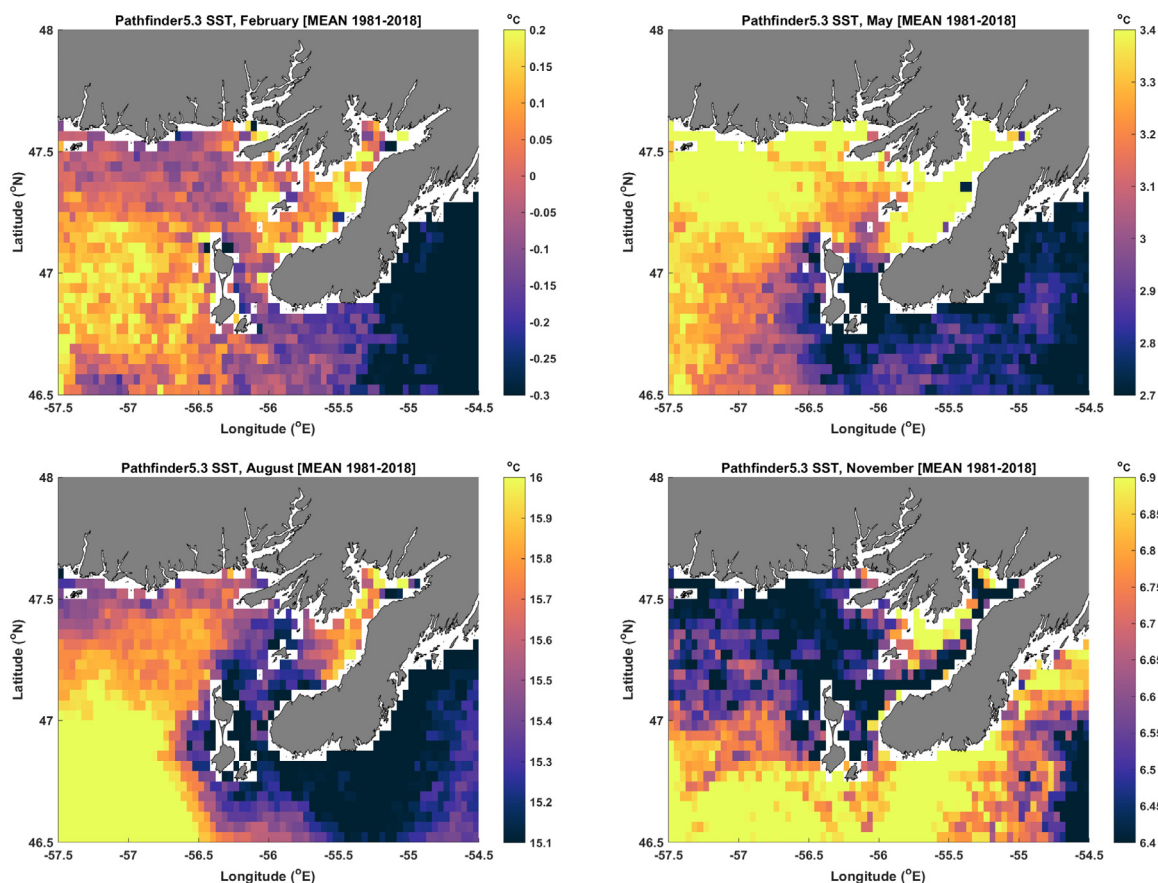
Fig. 4. SST climatology of months representing seasonal peaks. Colorbar ranges were set to be from mean-1 std to mean+1 std where std is the standard deviation associated to the mean fields presented.

southern shore of the Burin Peninsula during all seasons but fall. The colder water appears to generate from Placentia Bay at its southern offshore boundary, to travel through the Saint-Pierre–Burin channel in spring, extending northward in summer before spreading and veering westward, following the Newfoundland coast in fall. While the propagation pattern probably results from advection of cold water by the Labrador Current (Loder et al., 1998), the persistent area of cold water on the eastern side of the peninsula could, in part, be attributed to upwelling-favourable winds as shown by Ma et al. (2012); see also next section on wind showing prevailing southwesterlies from spring to fall). A cool area along the Burin Peninsula, in Fortune Bay, also appears in fall (November) but is difficult to interpret since it also corresponds to poor data coverage.

In the current context of rapid climate change, it is useful to get a sense of long-term SST trend. We calculated this trend for Fortune Bay by calculating annual means from the monthly averaged series used to create the monthly climatology described above. By using a linear fit on those annual means, a linear trend of 0.04 °C/yr was found, corresponding to an increase of 1.5 °C over the 37 full years of the observations (1982–2018; Figure S11). The same analysis was run on the monthly averaged series to evaluate the potential seasonality of this trend. Monthly trends are larger than the annual trend from July to November and lower in the other months (Figure S12). It peaks in August with a value close to 0.07 °C/yr and is the lowest in June at about 0.03 °C/yr. These results suggest an increase in the potential for summer heatwaves and a comparatively weaker decrease in the potential for winter superchill (i.e. sub-zero temperatures).

Watershed areas and runoff into Fortune Bay were estimated in Donnet et al. (2018b). As only one river, Bay du Nord river

(BDNRI, Figure 1) has been monitored (and continues to be) by ECCC (https://wateroffice.ec.gc.ca/search/statistics_e.html, station 02ZF001), the inputs from all the other rivers to the region were estimated from it, i.e. using area ratios (see Donnet et al., 2018b for details). BDNRI's discharge presents two peaks: a main one in April corresponding to the 'spring freshet' ($\sim$70 m^3/s average) and a smaller one in November–December ($\sim$50 m^3/s average); its lowest rate occurs in summer ($\sim$20 m^3/s in July–August) and its annual average is about 40 m^3/s (Fig. 5). Using those data, the total annual mean runoff to Fortune Bay was estimated at 163 m^3/s with a peak at 280 m^3/s in April, a low at 80 m^3/s in July–August and a second peak at 214 m^3/s in December; about 4 times BDNRI's output.

The effect of freshwater inputs on the bay's stratification, i.e. its change in salinity, can be looked at by comparing these inputs with the salinity climatology presented earlier and with near-surface salinity timeseries data recently collected (Donnet et al., 2020). We used BDNRI's monthly climate discharge described above and monthly climate of salinity at 5 m depth presented in Fig. 2 to make a 'climatology comparison' (Fig. 5) while BDNRI's monthly average timeseries were used for comparison with the recent timeseries collected from oceanographic moorings (Fig. 6). Four moorings were deployed during two full years (May 2015 to May 2017) with a CTD moored within the first 2–16 m. The timeseries were filtered using a moving average with a window of 30 days to remove the high frequency signals and get a better picture of the seasonal cycle.

The spatial transition from oceanic waters of the shelf (WOA series) to the coastal ROFI of Belle Bay (BB series) is once again evident with salinities decreasing by about 0.2 g/kg in winter (February) to more than 1 g/kg in summer (August) from WOA
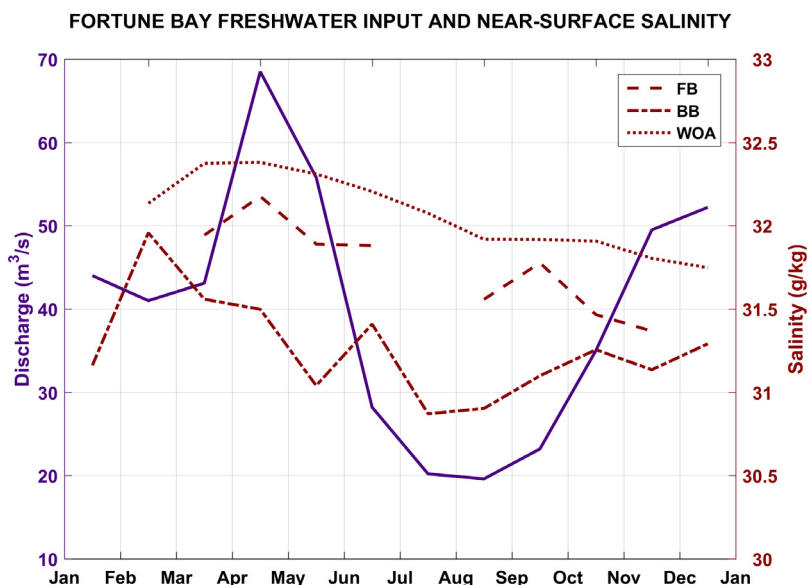
FORTUNE BAY FRESHWATER INPUT AND NEAR-SURFACE SALINITY

Fig. 5. Bay du Nord River discharge and Fortune Bay near-surface salinity climate (FB and BB polygon areas).

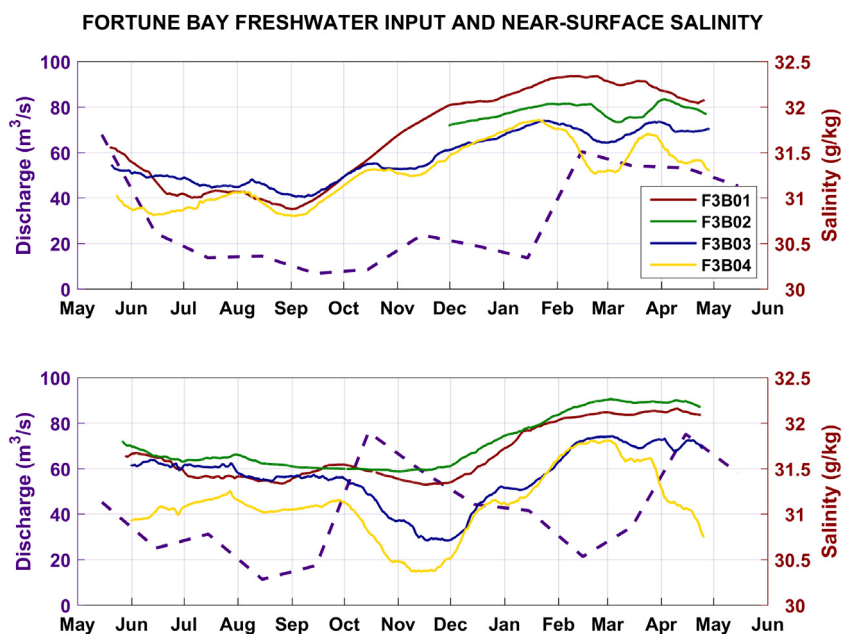**FORTUNE BAY FRESHWATER INPUT AND NEAR-SURFACE SALINITY**

Fig. 6. Bay du Nord river input (dashed) vs. near surface salinity measured at F3B01 (red), F3B02 (Green) in FB and F3B03 (Blue) and F3B04 (Gold) in BB. Top panel is the 2015–2016 period while bottom panel is the 2016–2017 period.

to BB (Fig. 5). FB values lie roughly in the middle as a transitory region. Considering standard deviations of the order of 0.2 g/kg, 0.3 g/kg and 0.2 g/kg for FB, BB and WOA, respectively, there are some overlap amongst the series, however. BB's near-surface salinity cycle appears to be almost in phase with the freshwater discharge, that is: high values in winter and low values in summer. April and November–December peaks of discharge do appear to have a small effect, lowering the salinity in May (thus, one month after) and November, but the lowest values seen in July–August seem at odds with a locally forced system.

The timeseries comparison, Fig. 6, confirms the low frequency salinity cycle with a low in summer and a high in winter (more visible in 2015–16) although the cycle appears to be modulated by higher frequency 'freshening events' in BB (F3B03&04 series of November, March and May, in particular). Those events appear

to be in phase or occurring just about a month after a peak of river discharge. It should be noted that the interpretation of these data is complicated by the uneven vertical distribution of the observations. The freshening lag seen between F3B03 and F3B04 in February–March and November 2016, for instance, might be due to the deeper measurement made at F3B03 during these time periods (16 m vs. 5–8 m at F3B04). Important interannual variability was observed also, with a difference of about 0.5 g/kg observed between the summers of 2015 and 2016.

We consulted the latest Sea Ice Climatic Atlas to assess Fortune Bay's ice climate (Canadian Ice Services , CIC). The maximum frequency of occurrence of new ice in Fortune Bay from this atlas is 1%–15% during the weeks of February 26, March 12 and March 19 (to a much lesser extent for the latter); thus a total of 3 weeks over the November 12–August 27 period reported by

the atlas. This frequency of occurrence is calculated over a period of 30 years (1981–2010); so that sea ice would be observed in Fortune Bay about once every 7–100 years. Local knowledge reported in de Young (1983) indicated that ice presence in Fortune Bay is very seldom other than in small harbours and coves and that advected ice from the Gulf to this region can occur in late winter to early spring of heavy ice years. Our discussions with finfish farmers and local fishermen during our own monitoring program (2015–17) led to the same observations.

5. Wind

Monthly wind roses as well as general characteristics of the wind climate of the Fortune Bay region was recently presented by Donnet et al. (2018b). For the purpose of this paper, the analysis was extended using a slightly longer timeseries available (25 yrs vs. 20 yrs) and a focus was given on forcing aspects that are thought to be important to the ocean dynamics (and response) of the embayment, i.e. directionality and frequency of occurrence of strong events.

ECCC weather station hourly data from Sagona Island (SAGIS, Figure 1) were downloaded from February 1994 to January 2019, covering 25 years but with significant gaps. In total, about 3 full years (2008, 2014 and 2018) and about 19 other full months (June–July 1994, June–July 2001, February–March 2002, April–July 2002, July–August 2005, March–September 2011 and February–August 2015) are missing from the timeseries. The data was further reduced for more statistical robustness to include solely days with 16 or more hours of data and months with 20 days or more of data leading to a timeseries consisting of 7250 days and 238 months, corresponding to about 20 years of useable wind data. Wind speed values were also adjusted to 10 m above mean sea level before the analyses using the Large and Pond (1981) formula (from a measurement height of 70 m above mean sea level).

Seasonal wind roses are illustrated in Figure S13; showing the annual cycle in both speed and dominant direction. Overall, prevailing winds are from the west, as expected for the region, but strong winds can come from any direction and spring and fall winds are more variable. Computing a monthly wind speed climate from the hourly timeseries (same method than with the AT), it was found that there is a factor of almost two in wind speed between the windy month of January (10 ± 1 m/s average) and the more gentle month of July (5.5 ± 0.5 m/s average).

Given the orientation of the Fortune Bay–Belle Bay system, wind blowing along the main axis of the bays, i.e. from the SW and NE (along FB), SE and NW (along Belle Bay) are expected to produce the largest oceanic response (e.g. in the form of upwelling or downwelling and/or sea level setup and setdown). To illustrate the seasonal change in direction, a monthly percent of occurrence wind direction plot was made using the four main axes directions mentioned above and using full quadrants (e.g. 0–90°N range for NE winds) (Fig. 7 A). The strong seasonal variation in wind direction is evident from this latter plot with a clear shift from prevailing NW winds in winter to prevailing SW winds in summer.

To get a sense of the frequency and importance of wind forcing on the embayment, a persistence analysis was carried out. The same four main directions described above were chosen for the analysis along with a wind speed value of 10 m/s. The number of events with wind blowing for a duration equal or superior to 6 h, 12 h, 18 h and 24 h were computed for each direction and each of the months of the timeseries and then averaged monthly to produce a monthly climate. The 6 h scenario is illustrated in Fig. 7B. Strong seasonality is again evident from this latter plot, showing frequent stormy conditions (> = 8 wind events lasting

6 h or more from any direction per month) from September to May, i.e. 2/3 of the year. From June to August, a much calmer period occurs (2–5 events from any direction, per month). Same directional shift pattern (from prevailing NW to prevailing SW winds) is observed from this analysis. 12 h events are about twice less frequent than 6 h ones with northerly winds (NE and NW) and 3 to 5 times less frequent with southerly winds (SW to SE, respectively). Wind events equal to or larger than 18 h in duration occur 5 to 10 times per year, on average (NE and SW winds and NW winds, respectively). Events equal to or larger than 24 h in duration are rare (1 occurrence of NE and SW winds; 5 occurrences of NW winds, on average per year).

6. Tides

Analyses of tides of the area were presented in Donnet et al. (2018b) and Ratsimandresy et al. (2019) who reported sea-level and currents characteristics, respectively. Both studies focussed on the inner part of the bay (Belle Bay) and used relatively short timeseries (usually a few months long), however.

The objective of this section is therefore to complete the previous studies using newly collected and longer timeseries (see Donnet et al., 2020 for details) and by examining the importance of the non-tidal component of the sea-level. Information on the tidal currents vertical structure and seasonal variation will be offered in the next section along with the non-tidal components of the circulation.

A tide gauge is installed at the head of the Belle Bay, on the wharf of Pool's Cove since May 2015, recording sea-level and water temperature at 10 min interval (see Fig. 1 for location). The gauge has been continuously maintained since its deployment but has suffered from a number of sensor failures, resulting in gaps in the timeseries. The longest continuous record available, from May 2015 to March 2016 (331 days), was used for analyses.

Tidal constituents were first extracted from the series using the T_Tide harmonic analysis programs (Pawlowicz et al., 2002). Residual (non-tidal) water level variations were subsequently calculated by subtracting the determined tidal signal from the original series. A wavelet analysis was finally performed to determine the periods of potential transient signals in the residual series using Grinsted's wavelet coherence programs (Grinsted et al., 2004). The original record along with the results of those analyses are presented in Fig. 8. The major constituents are M2 (0.65 m), S2 (0.18 m), N2 (0.14 m), O1 (0.07 m) and K1 (0.07 m); leading to a form factor F (K1+O1/ M2+S2) equal to 0.17. Tides in Fortune Bay can therefore be defined as semi-diurnal (Courtier, 1939). As seen in Fig. 8, the tidal range is about 2 m at spring tides and 1 m at neap tides.

Residuals account for only about 4% of the raw signal variance but can have substantial magnitude (order of 0.5 m). Those notable events are transient in nature but more frequent and stronger in fall-spring (October to April). Wavelet analysis indicates that those events have periods of 1–2 days generally and sometime longer (4–5 days). A Butterworth band-pass filter analysis performed on this 1–5 d band indicates that those events can have an amplitude of the order of 10–30 cm. At higher frequencies, frequent signals occur in the 0.125 day (3 h) and 0.02 day (0.5 h) bands which are close to Fortune Bay and Belle Bay's natural mode 1, respectively (about 2 h using a 130 km long Fortune Bay and about 0.5 h using 30 km long Belle Bay; both 160 m depth). This latter observation indicates frequent occurrence of seiche activity particularly during the late fall to early spring when numerous strong wind events occur in the region. A 0.014–0.25 d (20 min to 6 h) band-pass filter revealed amplitudes of those seiche to be of the same order of magnitude as the low frequency signals (1–5 d band). Given a 10 min sampling of the timeseries, however, aliasing effects can also be expected. Some signals also occur within the 0.5 d band which may be due to the imperfection of the tidal analysis.
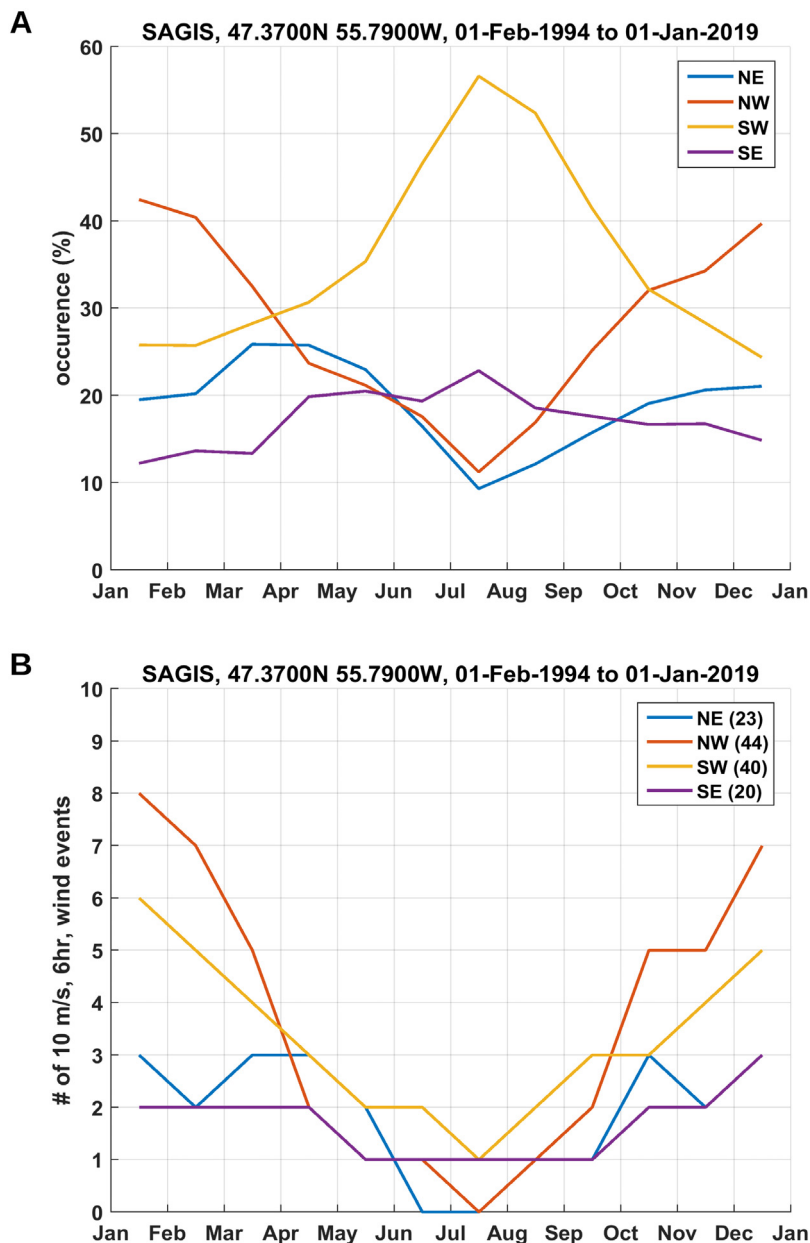
A

SAGIS, 47.3700N 55.7900W, 01-Feb-1994 to 01-Jan-2019

B

SAGIS, 47.3700N 55.7900W, 01-Feb-1994 to 01-Jan-2019

Fig. 7. Wind direction (From) monthly climate from SAGIS along the four main axes of the Fortune Bay–Belle Bay system (A). Persistence of 10 m/s wind blowing 6 or more hours along the four main axes of the Fortune Bay–Belle Bay system; total (annual) number of events for each direction is given in bracket in the legend (B).

7. Currents

Currents in the inner part of bay (Belle Bay) were assessed statistically for 2 layers (0–20 m and 20 m to sea-bottom) in Ratsimandresy et al. (2019) using a number of ADCP records collected at various locations, principally near aquaculture sites.

The objective of this section is to expand the previous work by providing more information on the vertical structure and temporal variation at seasonal scale for the bay as a whole as well as providing quantitative estimates of the dominant energy bands using recently collected and longer ADCP timeseries (see Donnet et al., 2020 for details).

7.1. General characteristics

An example of current speed and direction series, taken from May 2015 to May 2016 is presented in Fig. 9. These observa-

tions were obtained from two upward looking ADCPs (300 kHz) mounted on the same line at about 55 and 150 m; low scattering conditions resulted in small data gaps between 50 and 70 m. The main features of this series are representative of the region, that is: stochastic 'events' appearing more frequently from October to March and a directionality dominated by low-frequency oscillations (N–S in Fig. 9). Effects of stratification is more evident during the summer season (July-September) with localized 'pulses' towards the surface though signs of layering processes, i.e. changes of direction with depth and maximum speed dipoles on the vertical, appear throughout the year. Strong, near-bottom to mid-depth (50–100 m from bottom) events also occur frequently during the fall to spring season (late October–early May).

7.2. Seasonal statistics

To get a sense of the seasonal variability, some basic statistics were calculated by time-averaging the ADCP profiles seasonally
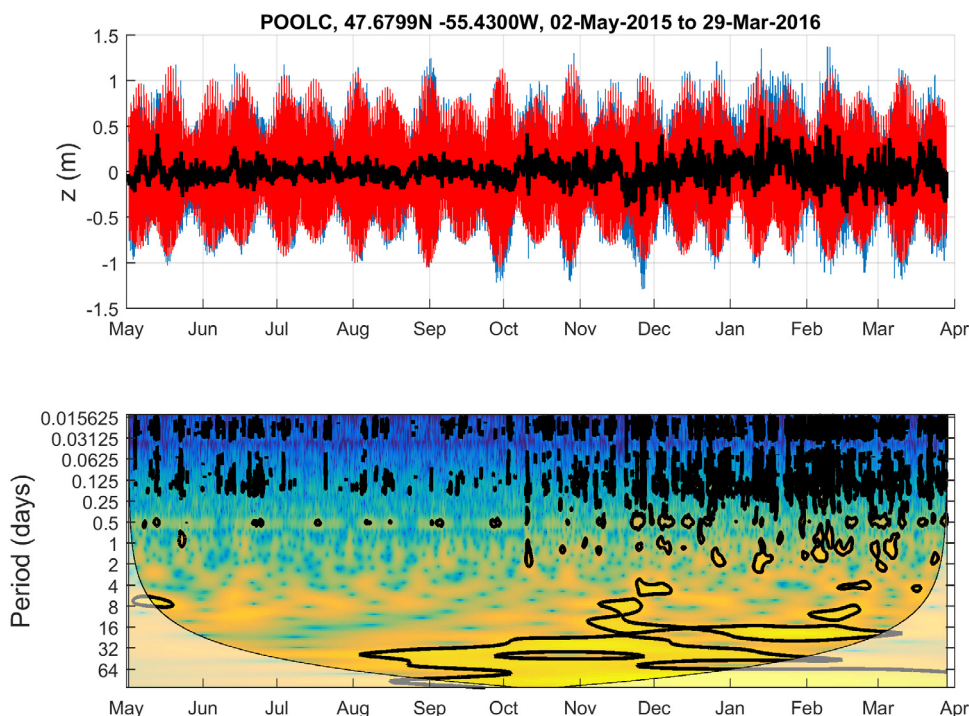
Fig. 8. Sea level record (blue), tide (red) and residual (black) at POOLC (Belle Bay), top; residual wavelet analysis, bottom. On the wavelet plot, the thick black contour designates the 95% significance level against red noise and the cone of influence (COI) where edge effects might distort the picture is shown as a lighter shade.
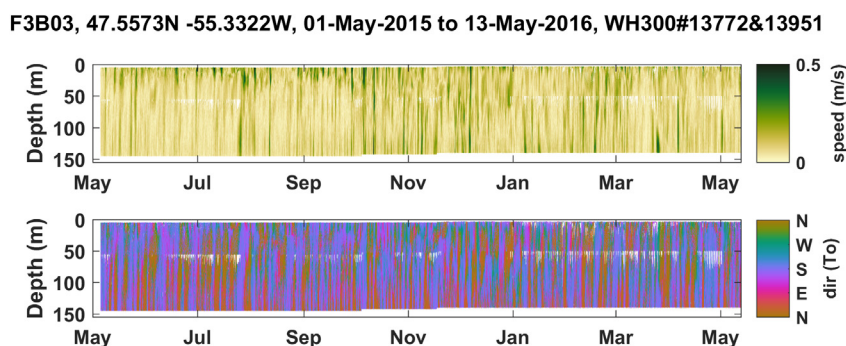

Fig. 9. Ocean current speed and direction observed at the mouth of Belle Bay (west side; see Fig. 1 for F3B03 location, site depth = 155 m).

(see Figure S11 for a representative example). The analysis was performed using the observations made from May 2015 to May 2017 at 12 locations around the bay (F3B01-12, see Figure 1 for location and Donnet et al., 2020 for details). Overall, mean current speeds are about 8 ± 5 cm/s, maximums are on the order of 40 cm/s and both vary, on average, by a factor of about 2–2.5 with depth and a factor of about 1.5 seasonally at any given site (2–20 cm/s range, altogether for the means, 10–90 cm/s range for the maximums). The strongest currents are usually found near-surface (upper 20 m) and the weakest towards the middle of the water column (F3B02&03) or near-bottom (F3B01&04 and all sites <100 m depth). Maximums were also found in subsurface (20–60 m) at some sites (F3B01, 03, 04 and 05) in fall. Seasonally, the fall period is the most dynamic while the spring is the least dynamic (closely followed by the summer). Spatially, currents are stronger in the outer part than in the inner part of the fjord by about 50%, on average, in mean speed. Large spatial variability is, however, to be expected given the region's complex bathymetry.

7.3. Seasonal circulation

Vector averaging the currents at 10 (1.5 at F3B12), 70 and 135 m depth, a seasonal picture of the mean circulation was obtained (Fig. 10). We define those depths as representative of 'surface', 'middle' and 'bottom' layers, respectively, taking the hydrographic structure presented above into account. Note that 135 m, the deepest level we could use from our data, is probably a little too shallow to be fully representative of the bottom layer. Indeed, a depth of 200–300 m would be more appropriate to represent the bottom layer and its processes as shown in de Young (1983) and Hay and de Young (1989). Similarly, 70 m is a little too shallow to be representative of the intermediate layer in fall but was the deepest available data from the moorings F3B05-11. The maps presented in Fig. 10 are a composite using the 2016–17 surface and mid-depth observations and 2015–16 bottom currents at all sites but F3B01. Due to data gaps in current direction, we used data from the 2015–16 observations at all depths for the spring, summer and fall periods and used data from
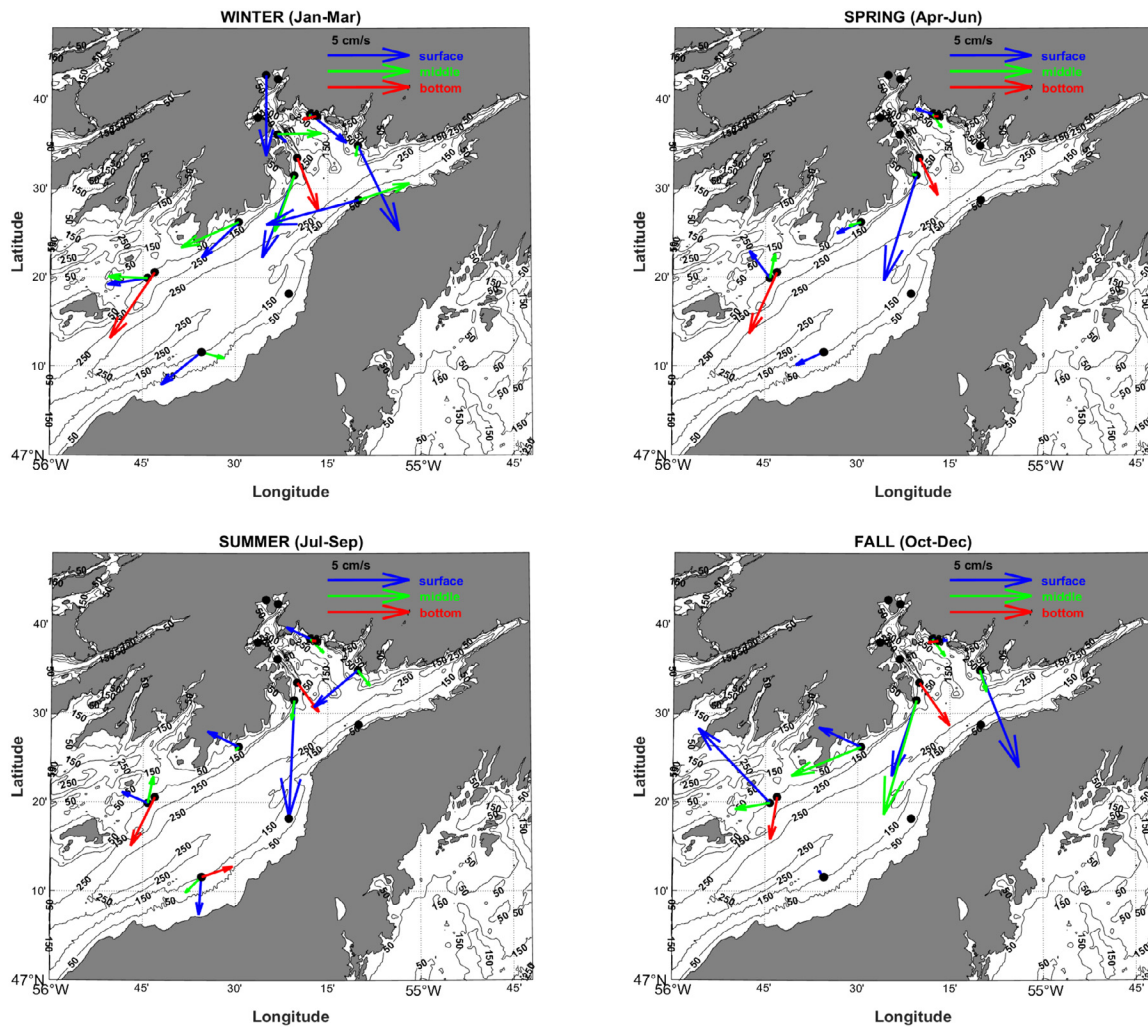
Fig. 10. Mean, seasonal, circulation near-surface (10 m), middle (70 m) and near-bottom (135 m) layer. Scaling by a factor of 3 was applied to near-surface currents at F3B12 (winter) due to their much larger magnitude.

the 2016–17 observations to represent the winter period surface and mid-depth layers for this latter site. Except for F3B02 in spring, the results were coherent over the 2 years of observations. At F3B02, surface currents flowed towards the SW in spring 2015 (as opposed to the NW in 2016) and mid-depth currents towards the W (N in 2016); currents were about the same strength at the near-surface level in both years but much weaker at mid-depth in 2015 (about 3 times less). Mean circulation is rather weak, on the order of 1–5 cm/s except in the Bay du Nord river estuary (F3B12) where mean surface outflow is about 15 cm/s in winter (factor 3 scaling applied in Fig. 10's arrow). The near-surface flow is oriented outward the bay at all sites and seasons except at F3B04 where it is inward in spring and summer. Flow is roughly oriented the same way at mid-depth except at F3B01&11 in winter where it is in opposition (inward). Bottom currents are not shown at F3B01 for the winter, spring and fall seasons due to a lack of current direction observations, reducing the coverage below the 80% seasonal representativeness threshold chosen. For the same reason, currents are not represented at F3B05 (all seasons) and F3B07 in spring and fall. F3B11 was deployed only from November 2016 to May 2017 and from June 2016 to May 2017 at F3B08, reducing the coverage to the winter at F3B11 and to the winter, summer and fall seasons at F3B08, using a 80% threshold. Using all the data available, a moderate near-surface inward flow appears in spring and a strong near-surface outward flow appear in fall at both F3B08 and F3B11. At mid-depth, flow

is outward at F3B08 and inward at F3B11 in both spring and fall, however, while being rather strong in fall (∼5 cm/s) it is very weak in spring (<1 cm/s) at F3B11. At F3B01, bottom currents are inward in both spring and fall (see Figure S12 for an illustration).

7.4. Spectral analysis

To investigate the higher frequencies, a spectral analysis was carried out. The analysis was done on the dominant along-shore component (about 2-2.5 times larger, on average, than the cross-shore component) at each mooring site described above and for the same depths as those of the mean circulation maps analysis presented above (i.e. 10, 70 and 135 m). We used a classic Fast Fourier Transform (FFT) algorithm following the Welch's method with a 85-day half-length overlapping Hanning window (4 degree of freedom over a one year timeseries) to perform the analysis. Selected illustrations are presented in Fig. 11; only results from moorings F3B01-04, year 1, are presented as they were found to be representative of the region and observed period (2015–17) as a whole. In general, the spectrums are red with a large plateau at low-frequency ending around 0.5 cpd (2 days period) followed by a sharp decrease and a prominent peak corresponding to the semi-diurnal tides (with a notable exception at F3B04). No significant peak at the inertial frequency (1.47 cpd) was observed at any of our monitored sites. At high frequencies, from about 10 cpd (2.4 h period), the surface layer spectrum (10 m) falls off rapidly
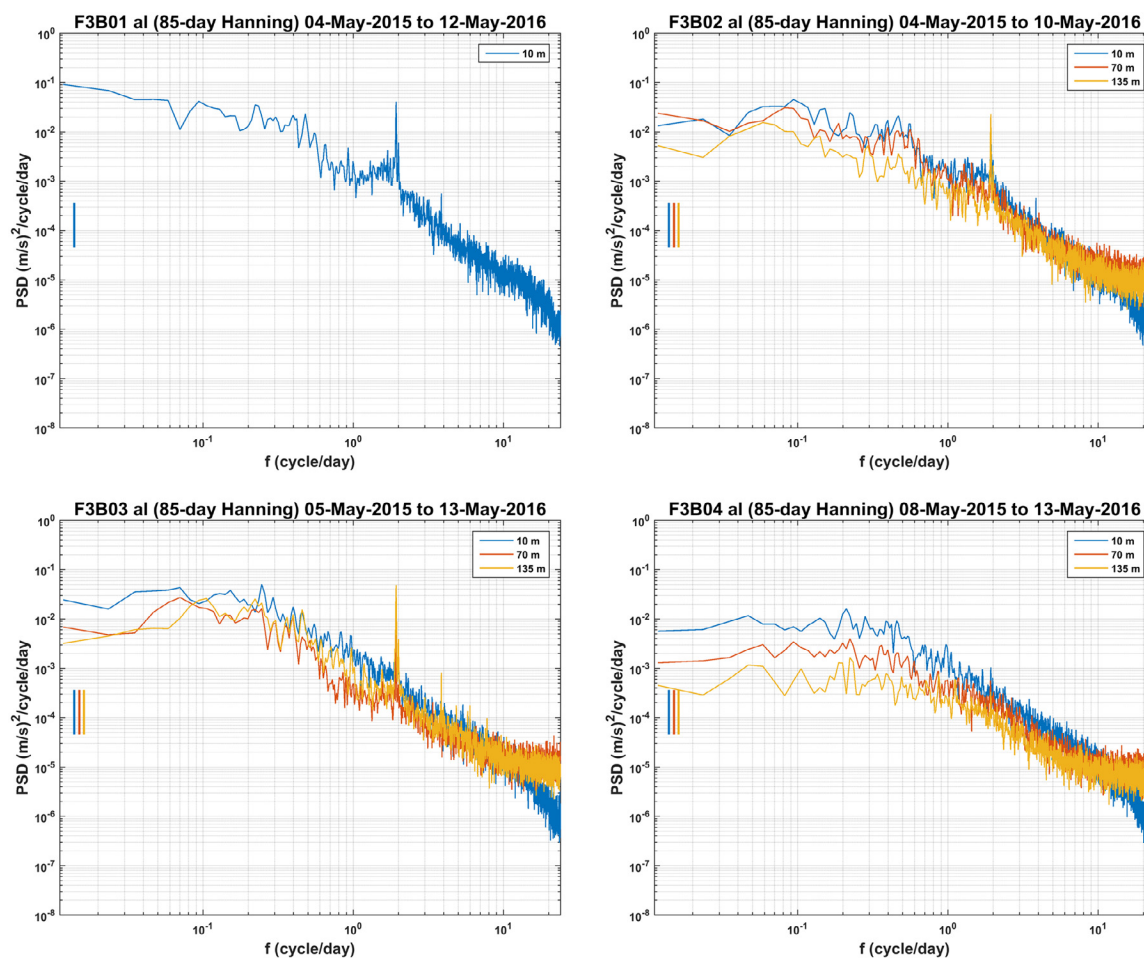
Fig. 11. Annual spectrums of the along-shore current component at F3B01-04 sites (F3B01&02 in FB, F3B03&04 in BB). 95% confidence interval of each spectrum is represented by a vertical bar on the left hand side of each plot. Note that because of mooring deployment issues, F3B01 along-shore currents at 70 and 135 m depth are not available.

while deeper levels spectrums (70 and 135 m) tend to flatten at all sites. From the inertial frequency to the 10 cpd inflection point the slope was found to be −2 on average (−2.7 to −1.7 range). While this slope is consistent with the Garrett-Munk spectrum model of internal waves (Garrett and Munk, 1972, 1975), the latter was developed using open-ocean data. This suggests that energy dissipation due to internal waves may exist in Fortune Bay in a similar way than in the open ocean. We can also note the departure from this slope at higher frequencies (10 cpd) where the spectral energy falls off near the surface while it flattens at depth. This is at odds with the findings of Levine et al. (1983) which showed flattening of high frequency energy to happen in the upper part of the ocean and suggest intensification of internal processes near the bottom rather than towards the surface in Fortune Bay. F3B06 spectrums are similar to those of F3B03 and F3B08 are similar to those of F3B04. F3B11 resembles that of F3B04&08 with a more discernible peak at semi-diurnal frequencies. Integrating under the spectrum, we estimated the energy of three main bands, 2–20 d (low frequency, or 'weather band'), 6–30 h ('tidal band') and 2–6 h ('high frequency' band) expressed as a variance, and compared it with the total signal (by computing a % ratio). We also used a 5th order Butterworth band-pass filter to check and complete the analysis at all depths and found the same results. The distinction between those bands were based on visually inspecting variance preserving spectrums (not shown) for the weather band and by assuming that most of the tidal energy would be restricted to the diurnal to quarter-diurnal band. The

high frequency band was defined as simply being anything of higher frequency than the other 2 bands. Overall, the weather band contributes to half or more of the total signal variability (47% on average, 20%–63% range across all depths and sites) while the tidal band contributes to about 20% (9%–34% range) and the high frequency band accounts for less than 5% (1%–14% range) only. Expressed as RMS (Root Mean Squares), the weather band currents are found to be about 6 cm/s, on average (1–12 cm/s range), the tidal band current about 3 cm/s average (1–6 cm/s range) while the high frequency currents are only about 1 cm/s on average (1–3 cm/s range) for a total signal of about 8 cm/s (2–16 cm/s range). It should be noted that the tidal band used here is rather large and probably includes energy from other processes than the tide. Similarly, the low frequency and high frequency bands may include tidal harmonics of lower or higher periods than the, assumed, dominant diurnal to quarter-diurnal band.

7.5. Weather band

Pulses of current characterize the weather band and appear more transitionary in nature than periodic (explaining the rather flat PSD distribution in the spectrum). A couple of examples of these pulses using the along-shore component are presented in Fig. 12. Along-shore currents are defined as being positive for a flow going into the bay (red colour), i.e. northeast-ward in the outer part and northwest-ward in Belle Bay, and negative (blue colour) for an outgoing flow. Top panel of Fig. 12 illustrates the
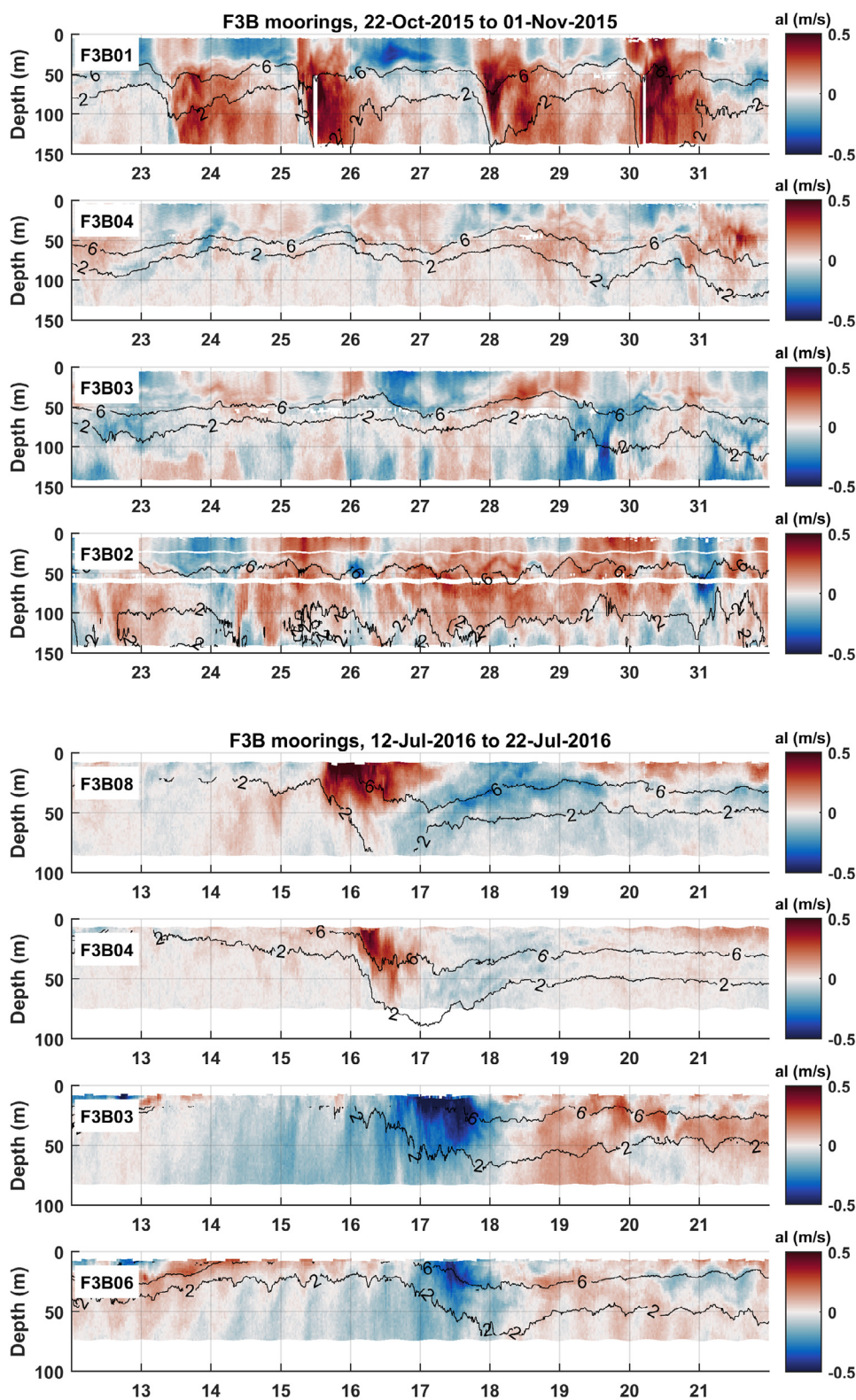
Fig. 12. Fall (top) and summer (bottom) along-shore current events observed around Fortune Bay (see mooring location in Fig. 1).

frequent occurrence of those events affecting most of the water column during the fall season while the bottom panel shows an example of the more sporadic occurrence of those events taking place over a more restricted portion of the water column (upper 50 m) in summer. In both cases, the response appears

coherent, progressing around the bay in a cyclonic motion (F3B01 to F3B03 in the fall illustration, F3B08 to F3B06 in the summer one). In the fall example, 4 large pulses occurring 2–3 days apart (23, 25, 28 and 30th of October) are clearly visible at F3B01 (FB, southernshore). Currents of about 0.5 m/s associated with

isotherms vertical migration of the order of 25 m to 100 m (6 °C and 2 °C isotherms, respectively) characterize those pulses. Interestingly, while the inflow appears principally barotropic in nature (i.e. currents going in the same direction with depth), the outflow are clearly baroclinic with a current inversion occurring around 50 m depth. Though much less energetic and more baroclinic in nature, those four pulses occur at F3B04 and F3B03 with about half the flow speed, less vertical migration of isotherms (10–50 m) and 1 and 1.5 d delay from F3B01, respectively (as an upper layer outflow at F3B03, in October 25, 26.5, 29.5 and 31.5). F3B02 stands out from the other sites with relatively strong currents but varying less distinguishably as pulses and showing a more stable 6 °C isotherm. The latter is subject to semi-diurnal signals, however, of about 5 m amplitude, which are probably of tidal origin. The cyclonic propagation is more visible in the summer example with a large downwelling (50–100 m range) associated with strong currents (∼0.5 m/s) occurring at all sites around Belle Bay (F3B08, 04 and 03) and on the northern shore of FB (F3B06). Not shown (no along-shore current data), F3B01 and F3B05 also experienced a strong downwelling event (almost 100 m for the 2 °C isotherm), occurring about 2 days earlier than at F3B08 (July 13). Similar to the fall, F3B02 (not shown) appears uncorrelated with the other sites with the exception of a rising and falling 2 °C isotherm during the downwelling and upwelling phase observed at F3B01 from the 13 to the 16 of July.

Results of cross-correlation analyses (see details in the supplementary materials) show that those pulses are well correlated amongst most sites both in terms of isotherms (June–December) and along-shore currents (throughout the year). The correlations are stronger amongst mooring pairs from F3B08 to F3B06 and the lowest with F3B02 and their lags consistently indicate a cyclonic propagation (as seen in Fig. 12). Using the correlation' lags and distance between mooring sites, we obtained phase speed estimates of 0.5–2 m/s, increasing from spring to fall.

Further statistics were calculated to get a sense of the frequency of occurrence, duration and excursion associated with those pulses (see the supplementary materials for details). Those latter analyses reveal the occurrence of 28 ± 3 pulses per year of 23 ± 12 h (ingoing or outgoing flow) and associated excursion of 10 ± 7 km, on average and across all sites. Seasonally, a peak of activity is found from September to December when 3-6 pulses of 24 h duration or more (in either direction) can occur at any given site (and depth) per month (i.e. about 1 event of 48 h duration every 5–10 d). These pulses are not necessarily balanced in term of flow strength and duration and may therefore lead to a net transport (at any given depth, or even vertically integrated). Net transports of up to almost 20 km, at any given depth, were found using timeseries presented in Fig. 12.

8. Inner bay water exchanges and flushing times

In the context of fisheries and aquaculture activities occurring in Fortune Bay, knowledge of water exchanges (and hence of flushing or residence times) is of primary importance. It has direct applications for a better understanding of issues such as larval retention (and dispersion), dissolved oxygen depletion (e.g. within finfish farms), finfish parasites dispersion (e.g. sea-lice) and virus outbreaks. Here, we will attempt to quantify the main exchange processes between the inner (Belle Bay), where the aquaculture sites are located, and outer part of the bay using the data presented herein and simple formulas that have commonly been used for estuaries and fjord environments (e.g., those used in Inall et al. (2015), in particular, which were applied to a broad fjord). Three main processes will be assessed: barotropic tide, estuarine circulation and the so-called 'intermediary circulation' (see Stigebrandt, 2012 for a review of those processes in fjords).

The water exchange rate estimates provided, Q (given in m³/s), correspond to the rate of water exchanged by a given process and the flushing time estimates, T (given in days), are based on the total amount of time necessary to renew the entire volume of interest (either whole basin or layer) from that process alone. Note that except for the barotropic tide, which takes place over the whole water column, T is evaluated for the replacement of the upper layers (surface and intermediate). Deep water renewal will be assessed separately based on previous studies findings.

8.1. Barotropic tide

A first estimate of Belle Bay's flushing time by the barotropic tide (T_{tide}) was given in Donnet et al. (2018b) using a simple version of the tidal prism method and led to a 70 d value. We will refine this first estimate using a slightly modified version of the tidal prism method proposed by Gillibrand (2001):

$$T_{tide} = (V + V_{tide})/(V_{tide}(1 - \lambda)) * Tp_{tide}$$

which includes a parameterization $(1 - \lambda)$ to account for the mixing efficiency of the return flow. V is the basin volume ($54,100.10^6$ m³, for Belle Bay at low water level), V_{tide} is the volume of water brought in and out of the basin by the tide (450.10^6 m³, using a mean tidal range of 1.4 m and Belle Bay area of 310 km² at mean sea level), Tp_{tide} is the dominant tidal period (12.42 h, M2) and λ is the efficiency parameter.

The original tidal prism method assumes complete mixing of the tidal volume during each flood and complete removal from the system during each ebb. This is highly unlikely in Belle Bay given the vertical stratification observed. λ account for the proportion of the flow that is being returned to the system during each flood tide (as volume of original water). Hence, $1 - \lambda$ account for the proportion of water that is being effectively recycled during each tidal cycle. A λ value of 0 would correspond to complete mixing and flushing, an unrealistic situation in Belle Bay, while a value of 1 would correspond to no mixing and flushing, also an unrealistic situation. Determining a suitable value of λ is difficult since it implies knowing precisely how much water gets mixed and gets flushed away, without coming back, during each tidal cycle.

Using a conservative approach and assuming that the fraction of water being effectively removed from the system during each tidal cycle would solely be due to the mean current determined earlier at F3B03 (Fig. 10), i.e. order of 5 cm/s year round for all layers, a λ value of 0.95 is obtained (i.e. $1 - (0.05 \, x \, Tp_{tide}/2/24500)$ where 24500 is the width of Belle Bay mouth, in meters). This would then lead to a flushing time of the order of 1255 d. While this latest estimate is likely overestimated, it might be closer to the reality of (barotropic) tidal flushing given the weakness of the tides acting in Belle Bay. Water exchange (or flushing rate, Q_{tide}) can be estimated using the tidal volume and period as:

$$Q_{tide} = Vtide(1 - \lambda)/Tp_{tide}$$

Which gives a range of 1.25×10^3 to $10 \, x \, 10^3$ m³/s ($\lambda = 0.95$ to 0, respectively).

8.2. Estuarine circulation

Net volume flux of the (fresh/brackish) surface layer, balanced by the (salty) lower layer of an estuarine circulation can be found using the Knudsen relations based on salt and volume conservation (see Burchard et al., 2018 for a recent review) which gives:

$$Q_{est} = (Q_f * S2)/(S2 - S1)$$

$$T_{est} = Vup/Q_{est}$$

Where Q_f is the freshwater discharge (71+39 = 110 m³/s annual mean, 35 + 19 = 54 m³/s to 121 + 67 = 188 m³/s range; August to April rivers discharge into Belle Bay + that of Long Harbour river, respectively; see Donnet et al., 2018b for details), S1 is the averaged surface layer salinity and S2 is the averaged lower (intermediate, in this case) layer salinity. V_{up} is the volume of the surface and intermediate layers (combined) estimated at $41,500.10^6$ m³ using a limiting sill depth of 210 m (separating Belle Bay from Fortune Bay). Simply interpreted, this relation means that, in a 2-layer ocean, the (surface) outgoing flow (Q_{est}) is balanced by the (subsurface) ingoing flow which is equal to the product of freshwater runoff (Q_f) with a salinity fraction representing entrainment of the incoming, salty ocean water by the fresh, surface flow (then becoming brackish as time and distance from the source increases). It assumes steady states and is applicable when S1 and S2 are not equal. S1 and S2 must therefore represent time-averaged conditions, i.e. representative of a mean flow. Due to entrainment, the outgoing flow is generally much larger than the freshwater runoff. Using a minimum of 29.5 g/kg (July) and maximum of 32 g/kg (February) for S1 and a constant value of 32.4 g/kg for S2, representative of our climatological conditions, we get a flushing rate range of 0.6×10^3 to 15×10^3 m³/s and corresponding flushing time range of 31 to 796 d. This range is large and reflects uncertainties as well as the strong seasonality observed in both freshwater discharge and surface salinities; with weakest flushing conditions in summer and strongest from fall to spring (i.e. when surface salinities are within 31–32 g/kg and Q_f >100 m³/s).

It should be noted that the Knudsen relations reflect averaged conditions, i.e. the net effects of all forcing, including those of wind and tides. As MacCready et al. (2018) recently showed, flushing processes are very closely linked and overall mixing inside the bay can be approximated via a modified Knudsen relation. Thus, equating Q_{est} with Q_{tide}, we could estimate values of λ which would be representative of the (averaged) inner bay mixing efficiency. Using the numbers used above lead to a λ ranging from <0 to 0.95. Negative values are unrealistic/unphysical and implies uncertainties in our data (either in our salinities such as S1 being too large or in our estimate of Q_f and/or tidal volume being too large or too low, respectively; the former being more likely than the latter two). Using yearly averaged values (S1 = 30.7–31.7, S2 = 32.4 where the range in S1 reflects near-surface and depth-averaged values of the surface layer, and Q_f = 110 m³/s) gives a λ of 0.5–0.8 and a flushing time of 94–229 d.

8.3. Intermediary circulation

The intermediary circulation was defined as being the circulation (i.e. currents) generated by density variations outside the fjord above sill depth (also called 'baroclinic pumping'; see Stigebrandt, 2012 for a review). An empirical formula quantifying this water exchange is given as Aure et al. (1996):

$$Q_{int} = \beta * \sqrt{(g * Bm * Ht * Af * \delta M / \rho_0)}$$

where β is an empirical coefficient (17×10^{-4}), g is the gravity constant (9.81 m/s²), Bm is the width of the mouth (24.5 km), Ht is the sill depth (210 m), Af is the horizontal area of the fjord (310 km²), δM is the vertical integral of water density standard deviation profiles taken outside the fjord from sea-surface to sill depth (25 kg/m² in spring, 28 kg/m² in summer and 37 kg/m² in fall; using FB's temperature and salinity data presented above) and ρ_0 is a reference density (1026 kg/m³). Using those values for FB (as 'outside fjord' forcing conditions) and Belle Bay (as the 'receiving fjord') we get a flushing rates of 33×10^3 m³/s (spring), 35×10^3 m³/s (summer), 40×10^3 m³/s (fall) and corresponding flushing times of 12–14 d.

It can be noted that this baroclinic pumping relation does not make any consideration to mixing nor to potential reflux of water at the mouth, which is unrealistic and certainly leads to an over-estimation (underestimation) of flushing rates (times). Yet, it can also be noted that those rates are 3-4 times larger than the rates estimated from the tidal forcing alone, even when considering the same assumptions of complete mixing and flushing for the latter (i.e. λ = 0; $Q_{tide} = 10 \times 10^3$ m³/s).

8.4. Deep water renewal

A timescale of 300 d was estimated by Hay and de Young (1989) for the cold LCW to replace all the bottom water (i.e. below sill depth or 120 m) of the bay as a whole. Since the renewal by this water mass only occurs for about half of the year (from May to December) it is unlikely that the LCW can renew the basin fully within a year. However, during the remaining half of the year (December to June), the basin is subject to renewal by the warm MSW which appears to renew it at about the same rate (as illustrated by their Fig. 11). As a result, it seems reasonable to expect a total replacement of Fortune Bay bottom water on a yearly timescale. This renewal has, however, distinct consequences on the properties of Fortune Bay's bottom water; on a semi-annual timescale. Other than the difference in physical characteristics of the two sources, one being cold (<2 °C) and the other being comparatively warm (>4 °C), these two water masses (LCW and MSW, respectively) are also very distinct in their chemistry. Hence, while the LCW is oxygen rich (>10 mg/L), the MSW is comparatively poor (<6 mg/L). As a result, the bottom water of Fortune Bay should experience a semi-annual cycle of not only temperature (warm in winter to spring, cold in late summer to fall) but also of dissolved oxygen (higher in fall, lower in spring). Latest available data, taken in months of May and November, thus representing spring and fall conditions, indicate that while the inner basin (located in Belle Bay) does exhibit lower DO concentration in spring than in fall, the outer basin does not. Considering the T–S characteristics, showing a rising in bottom temperature in November in the outer basin, and therefore indicating the onset of the warm, DO poor, MSW renewal season earlier than found in earlier studies, we interpret this result as due to a slightly longer residence time of the bottom waters in the inner basin (Belle Bay) than in the outer basin. Nevertheless, all considered, a yearly timescale for deep water renewal of both the outer and inner basin is probably the right order.

9. Discussion

9.1. Water structure

Fortune Bay's seasonally stratified, three layered, water structure is typical of a deep fjord separated from the shelf by a sill (see Farmer and Freeland, 1983; Inall and Gillibrand, 2010; Cottier et al., 2010 for reviews). The temperature and salinity climate of the fjord and adjacent shelf presented in this study (Fig. 2) highlights the result of 4 processes creating and destructing this seasonal stratification: atmospheric forcing, winter overturning convection, freshwater runoff and water exchange with the shelf.

The atmospheric forcing acts both as a stratification agent via solar radiation and as a mixing agent via wind stress. Thermal stratification starts in April and steadily increases until August after which the effect of atmospheric cooling and wind stress are indicated by a decrease in surface temperature and deepening of the isotherms. Surface temperature ranges from 0 ± 1 °C (February–March) to 16 ± 1 °C (August) while sub-surface (below 50 m depth) temperature stays below 2 °C for the most part of the year before increasing in late summer (September) by a few

degrees due to important surface mixing and decreasing back to an homogeneous 2 °C or less in January. Vertical gradient of temperature in the surface layer (0–20 m) is thus maximum in August with a rate of decrease of 0.5–1 °C per meter (larger in BB and smaller in FB). Untangling the effect of wind forcing vs. surface cooling in mixing the water column is difficult since strong cooling (Air–Sea temperature difference > = 2 °C) occurs at the same time as strong wind forcing (mean wind speed of 9 m/s or more); that is: from November to March. Nevertheless, given the large loss of heat observed (order of 15 °C at the surface) and the extent of the vertical mixing (order of 200 m or more) we suspect this (convective overturning) process to play a substantial role. We note that, unlike high-latitude fjords, this convective process would be due to cooling effect solely as sea-ice, when present, is limited to small side bays and coves subject to freshwater runoff (thus, not associated with a brine rejection process).

Freshwater runoff effect is most visible in BB; as expected for it receives more than 2/3 of all the freshwater discharge flowing into Fortune Bay (110 m^3/s vs 160 m^3/s annual mean, respectively). Freshwater runoff peaks in April (280 m^3/s) and December (210 m^3/s) and is the lowest in July–August (80 m^3/s) (Fig. 5); this is manifested by BB's near-surface salinity (upper 10 m) albeit with some phase delay. The lowest near-surface salinity of our climatology occurs in July, which suggests a slow propagation of the freshwater input from rivers mouths to the inner bay as a whole and/or reflects the combined effect of wind forcing (stronger from fall to spring) with summer heating on near-surface mixing (weaker in summer). We also observed an important interannual variability in river discharge (discharge peaked in May and February in 2015–16 vs. October and April in 2016–17; Fig. 6) as well as in near-surface salinity (June–September values about 0.5 g/kg higher in 2016 than in 2015, Fig. 6). Given the spatial reach of this latter variability (all sites affected about same way), it may have had more to do with shelf conditions (e.g. fresher in winter–spring 2015 or fall 2014) than from local river discharge, however. Important spatial variations between BB and FB and between FB and the shelf are also worth noting. While BB is characterized by a distinct and shallow (about 5–10 m depth) halocline present almost all-year round except from mid-winter to early spring (February–April), shelf waters show a clear seasonal cycle of higher salinity values (about 0.7 g/kg higher than BB within the upper 20 m, on average) with a much broader surface freshening occurring, gradually, over the upper 50 m from July to December (Fig. 2). This 'freshwater pulse' is a well-known feature on the Newfoundland Shelf which takes its origin much further North from a combination of sea-ice melting, outflow from the Baffin Bay and Hudson Strait and significant runoff from the Labrador coast (e.g. Loder et al., 1998). The pulse thus travels southwards with the Labrador Current and typically peaks in September at the long-term monitoring Station 27 located just offshore St John's (Myers et al., 1990). Assuming an advection rate of 0.1–0.2 m/s, a typical range given to the inner branch of the Labrador Current (e.g. Petrie and Anderson, 1983), this freshwater pulse should be seen about a month or two later in the vicinity of Fortune Bay, i.e. in October or November (∼450 km downstream of Station 27 when going into Placentia Bay and out; see Ma et al., 2012 for details on this bifurcation). The WOA climatological data presented here (south-eastern mouth of Fortune Bay) indicate a low in December (albeit without data in January, Fig. 2 and Fig. 5), suggesting a smaller advection rate; but our climatology of FB (Fig. 2) does show a significant drop in surface and subsurface salinity values in October (thus, more consistent with this advection rate) as evidenced by the large deepening of the 32 isohaline (from about 30 m to 60 m). In BB, about the same magnitude drop of the 32 isohaline is seen about

a month later, in November. The seasonal cycle of salinity differs also at depth (i.e. below 50 m) where a broad but distinct peak of salinity (S>32.5 g/kg) occurs from June–December on the shelf and is only apparent in September–October in both FB and BB; a much narrower period. This latter feature suggests an either limited advection of sub-surface water from the shelf to the fjord and/or important sub-surface mixing processes occurring within the fjord as previously reported by Hay and de Young (1989). The advective influence of the inner Labrador Current surface water on the other hand, seems to be limited to the outer part of the bay, for the most part, as illustrated by our SST climatology which shows a westward propagation of colder waters from May to November (Fig. 4). Nevertheless, our recent observations of near-surface salinity within the bay do show an annual signal (of about 1–1.5 g/kg range) that is most likely related to the shelf variability (Fig. 6). Taken all together, these different observations indicate that while the inner Labrador Current transport is the highest in winter and lowest in summer (Han, 2005; Han et al., 2008, 2011; Wang et al., 2015; Ma et al., 2016) and is of a sizeable amount of water (0.5–1 Sv upstream, offshore St John's, according to Ma et al., 2016), its influence on the water properties of Fortune Bay would be the highest during the summer-fall seasons and more important on the intermediate layer (50–150 m) than on the surface layer.

Overall, BB surface water appears to be directly affected by land-runoff and to slowly export its freshwater content during the summer before being subject to a significant vertical mixing in fall (Fig. 2). In contrast, FB appears to be a transitional region affected both by input of freshwater from BB (in summer in particular) and by input from the shelf (in late summer-fall in particular). The background shelf water (S>31.5 g/kg) would thus be modified by the local forcing and mixing in FB, lowering its salinity (by increasing its freshwater content) within its surface layer and at intermediary depth. Interestingly, Fortune Bay (as a whole) is also noticeably warmer than the shelf at both surface and sub-surface levels (by about 2 °C and 1 °C, respectively) as evidenced by both our temperature (Fig. 2) and SST climatology (Fig. 4) and this would suggest an either limited advection of the cold Labrador Current waters into the fjord again and/or the advection of warmer water going into (and mixing within) the fjord. While the difference of surface temperature may be due to the strongest haline stratification occurring in Fortune Bay (limiting vertical mixing at the surface and thus 'trapping' heat in the near-surface), the seasonal advection of deep MSW (below sill depth, in winter) described by Hay and de Young (1989) could be the source of warm water responsible for the difference observed at depth. Hay and de Young (1989) reported an increase of up to 2.7 °C at 420 m in winter (Dec-Jun) with peaks of 0.5-1 °C over 4 years of observations (Fig. 5 of their paper). A close look at our climatology points to a warming of the order of 1.4 °C below 300 m in FB, from a low of 0.1 °C in September to a high of 1.5 °C in April. As indicated by Hay and de Young (1989) the mixing of this warm water within the basin (during cold LCW summer renewal, in particular) must be important given the weak stratification that is found in our monthly averaged profiles (a rise of temperature only discernible below 300 m) and it would explain the warmer, sub-surface, temperatures observed in our climatology of Fortune Bay vs. that of the shelf (Fig. 2). Given the recent warming and deoxygenating trend of the MSW (Galbraith et al., 2021; Blais et al., 2021) it is conceivable that the deep and intermediate waters of Fortune Bay would follow a similar slope; although certainly much less important than in the Gulf of St Lawrence given the input and opposite effect of the LCW. On the long-term, i.e. last 37 years (1982–2018), the near-surface temperature of Fortune Bay has risen at a rate of 0.04 °C/yr. This is large in comparison to the global rate of 0.01

°C/yr found for a similar period (1971–2010; IPCC, 2014) but is comparable to recent estimates of the region (e.g. 0.04 °C/yr given by Belkin (2009) for the Newfoundland-Labrador shelf from 1982 to 2006 and 0.06 °C/yr given by Galbraith and Larouche (2013) for the NAFO region 3L – offshore St John's – from 1985 to 2012) and comparable to other areas such as the Mediterranean Sea (0.041 °C/yr) considered as a world 'hotspot' (Pisano et al., 2020). It should be noted that those estimates are sensitive to the period of observation as well as the dataset used/chosen; using the same period as that of Galbraith and Larouche (2013) the same trend (0.06 °C/yr) was found using our dataset. Nevertheless, and even at 0.04 °C/yr, the trend is substantial and can be expected to have important effects on the ecosystem. With this in mind, a monthly trend analysis was performed and indicated this recent warming to be driven up by summer months (July to November) which have warmed at a rate of up to 0.07 °C/yr (August) rather than by the winter months which show positive trends, nevertheless (0.03-0.04 °C/yr). This suggest that the probability for marine heatwaves may have increased but also that the probably for superchill events (i.e. subzero temperatures) may have decreased from 1982 to 2018; both conditions having negative effects on marine finfish aquaculture, for instance (Hargrave et al., 2005).

9.2. Mechanical forcing

Wind and tide (water level), the two main mechanical forces of coastal areas, were assessed statistically in this study to extract their main characteristics. Our results are consistent with previous studies (de Young, 1983; Donnet et al., 2018b) describing a strong seasonality of the wind regime (strong, 10 m/s average, northwesterly dominant winds in winter and mild, 5 m/s average, southwesterly dominant winds in summer) and small tidal ranges for a coastal region (2 m spring tides; 1 m neap tides).

The strong wind seasonality in direction reminds that of the Western European shelf as a mirror image (so called 'SOMA' cycle; Pingree, 1999) and, as for the European shelf, has a strong influence on the shelf and slope currents; notably by modulating the inner Labrador Current flow (stronger in winter, milder in summer; Han, 2005). The region is dominated by succession of extra-tropical storms (cyclones) which are particularly strong in winter (Plante et al., 2015). Plante et al. (2015) showed that most cyclones endured in Newfoundland travel from the southwest and rapidly intensify as they travel along the eastern North American coast (due to their interaction with the ocean, warmer in winter). Interestingly, they also found that cyclones are as frequent in summer as in winter, though much less intense during the former (see their Fig. 1, in particular). Overall, they counted an average of 7 cyclones per winter and summer season (3 months) and 6 cyclones per spring and fall season; that is about 2 cyclones or more per month all year round (26 in total per year). Our persistence analysis, which considered a wind speed threshold of 10 m/s, indicates that a duration between 12 h (49 events per year) to 18 h (20 events per year) would be necessary to correspond to this cyclones frequency. Considering a cyclone growth and decay over a period of about 4 days (Plante et al., 2015, Fig. 2) it appears that our 10 m/s threshold would correspond to the fully developed stage period of the typical storms occurring in the region.

Fortune Bay's water level variability is dominated by tidal fluctuation (96%) but residuals are large compared to the tidal range (±0.5 m setup±setdown; vs. 1–2 m tides). Our wavelet and band-pass filtering analyses of the water level indicate that those noticeable events are larger and occur more frequently from fall to spring and have associated periods of the order of 1–5 d. We attribute those events as the response to the frequent atmospheric disturbances occurring in the region which produce both local (inverse barometric) and remote effects (usually in the form of Continental Shelf Waves – CSW – as described in Tang et al., 1998; Thiebaut and Vennell, 2010; Han et al., 2012; Ma et al., 2015; Bezaud et al., 2020). The influence of those sea-level variations on the circulation could be important and will require further investigations.

9.3. Ocean currents

Currents are characterized by along-shore pulses travelling cyclonically around the bay and associated with important downwelling and upwelling (order of tens of meters scale) as illustrated in Fig. 12. An average of 28 ± 3 pulses of 46 ± 24 h duration (ingoing+outgoing flow) and having excursion length of 10 ± 7 km (ingoing or outgoing) occur in Fortune Bay per year. These pulses occur more frequently from September to December at most sites and affect most of the water column from 0 to 150 m (surface and intermediate layers). They appear also more frequently within the surface layer (0–20 m) along the northern and western shores from May to September (Figure S17). Given their frequency of occurrence, their scale (horizontal and vertical) and potential non-linearity (Figure S18), they may be an important source of transport within the bay.

Those pulses are well correlated within the bay, particularly from the northern to the western shore; suggesting efficient propagation of signals from the former to the latter (Figure S16). Lower correlation with the southern shore indicates that this part of the bay would be subject to other (or additional) processes, maybe influenced or induced by the shelf, or that signals either imported to or generated within the main basin would change characteristics (amplitude and phase) within the inner basin before travelling out. We found that the phase propagation speeds are on the order of 0.5–2 m/s, increasing from spring to early fall. These observations correspond relatively well with the 2-layer ocean theory of long internal wave propagation (e.g. Gill 1982, section 6.2) which gives a range of 0.4 m/s in spring to 1 m/s in summer with a 0.7 m/s value in fall using the hydrographic characteristics presented herein. These results resemble previous observations and modelling findings from two other large embayment of Newfoundland (Yao, 1986; de Young et al., 1993; Davidson et al., 2001; in Trinity Bay and Conception Bay — TB and CB, respectively, in Figure 1) which show the propagation of internal Kelvin waves along the coast of those bays during the stratified seasons. One can also note that the average number of pulses occurring in the bay corresponds to the average number of cyclones crossing the region (28 vs. 26, respectively), indicating a potential link between this regional atmospheric forcing and locally observed oceanic response which also be consistent with previous findings. This suggests regional similarities and importance of such processes on the coastal environment of Newfoundland (i.e. upwelling and downwelling propagation as long, coastally trapped, internal waves).

Compared to this 'regime of pulses' which is a part of the 2–20 d weather band, the tidal regime (~0.5–1 d) and mean circulation (>20 d) are rather weak. Mean tidal currents are about 3 cm/s and mean circulation is on the order of 1–5 cm/s. Statistically, mean pulses current speeds are about 12 cm/s (10 km excursion in 23 h). In general, pulses are seen as currents of about 20 cm/s or more in any given timeseries that we have worked with in this study.

Consequently, tidal excursion is very small compared to, albeit more stochastic in nature, pulses excursion: 1.4 km using a maximum tidal current of 10 cm/s, an upper bound value, vs. 10 ± 7 km for the pulses, on average. Evidences of internal tides were observed, on the other hand (Fig. 12), which have been commonly reported as being an important process in fjords' interior waters

mixing and preconditioning (e.g. for deep water renewal to take place; see Stigebrandt, 2012 for a review). Given the low level of energy at tidal and higher frequency bands observed in general, this process is unlikely to play a major role in Fortune Bay, however. Preconditioning is also not necessary for deep water renewal to occur in Fortune Bay due to its topographic and shelf's hydrographic particularities (three-basins system, see Hay and de Young, 1989 for details). Nevertheless, an understanding of the effect of this latter process on Fortune Bay's distinct interior water structure (compared to that of the shelf) would benefit from further investigations.

The results of the mean circulation presented in Fig. 10 are puzzling. They show a near-surface outgoing flow across the whole bay and along nearly all the seasons. An homogeneous out-flow of brackish waters is expected from narrow fjords where the flow is constrained by lateral boundaries. Fortune Bay, however, is wide (15–25 km for the most part) and one would expect to see the effect of the rotation on the flow of that brackish surface layer, i.e. a deflection to the right on side of river(s) mouth(s). Since most of the freshwater input to Fortune Bay occurs in BB, along the northernshore (about 2/3 Fortune Bay's total) and along the southernshore (from the Burin Peninsula; the remaining 1/3) one would then expect a cyclonic circulation to take place on the near-surface. This near-surface cyclonic circulation might occur from spring to summer as indicated by inflows at F3B11, F3B08 and F3B04 when using all available data (Figure S15) but it remains uncertain due to insufficient data coverage. Perhaps even more surprisingly, the outflow across all sites monitored and seasons (fall to winter, in particular) is also apparent further at depth (70 m) suggesting a return flow present either deeper or in the middle of the bay (as volume conservation prescribes). Using all data available again, a sub-surface (70 m) return flow appears from fall to winter on the southern shore (F3B01&11), however. Likewise, the effect of the Labrador Current, which should appear as an inflow along the southernshore is not visible, suggesting little influence of this otherwise major regional feature from the adjacent shelf on Fortune Bay's upper circulation. Deeper, at 135 m, the circulation appears cyclonic and more in line with previous knowledge and expectations, i.e. deep water inflow from the Saint-Pierre sill and from the Miquelon sill flowing northward and subject to earth rotation and topographic steering (de Young and Hay, 1987; Hay and de Young, 1989). This deep influx could also account for the upper outflow.

9.4. Water exchanges

Three main mechanisms of water exchange (flushing) between the inner and outer part of the bay were assessed, that is: barotropic tides, estuarine circulation and baroclinic pumping. Large ranges of flushing rate were found, reflecting both large uncertainties with the approaches as well as a strong seasonal variability (as reflected by the salinity climate). The effect of baroclinic pumping process appears to dominate the exchanges but this result should be tempered by the important limitations and assumptions involving the estimates. Hence, the method used to quantify the effect of baroclinic pumping process on water renewal is based on empirical data collected on the Norwegian shelf which may not be representative of our region. As stated by Aure et al. (1996), the empirical coefficient β depends on the distribution of the (baroclinic) forcing frequency which is probably area-specific. For fjords wider than their internal Rossby radius, which is our case, they also state that the transport would be reduced. Perhaps more importantly, the method assumes complete advection and does not consider the effect of mixing efficiency (or lack of) nor that of a return flow which are both likely and which can be significant; particularly for short-term events such as illustrated in Fig. 12. Finally, all the processes are very likely closely linked in the real world, as was demonstrated by MacCready et al. (2018) with the tidal and estuarine circulations. All together and since the Knudsen formulas provide with a net result from all the processes, they probably offer the most reliable estimates. Using those formulas and annual mean values of salinity and runoff, a complete flushing of the upper layers of Belle Bay is expected to take on the order of a few to several months.

10. Conclusion

We provided a physical oceanography overview of Fortune Bay, a broad fjord located in mid-latitude (47.5°N) on the southern shore of Newfoundland, a large island of eastern Canada's shores (Fig. 1). Fortune Bay can be defined as a fjord for being a deep embayment, carved by glaciers and surrounded by a series of shallower sills (Fader et al., 1982). It can be qualified as 'broad' in the sense that it is wide (15–25 km) with respect to its internal Rossby radius (5–10 km), an horizontal scale of motion determining, for example, the extent of cross-shore coastal upwelling excursion.

In many regards, Fortune Bay is similar to higher latitude Arctic fjords: it is deep, broad, strongly stratified seasonally, probably subject to important winter convection overturning (although not saline) and to important exchanges with the shelf (particularly with respect to deep water renewal) and is dominated by wind forcing for processes such as surface and subsurface circulation and vertical mixing. However, Fortune Bay is notably different from Arctic fjords by its large absence of sea-ice processes, absence of katabatic winds (although similarly subject to strong along-shore winds from regional cyclonic activity) and by an influx of a cold intermediate water masses instead of a relatively warm one for many known Arctic fjords. In this sense, Fortune Bay could perhaps be defined as a 'broad, sub-Arctic fjord'. Two other important topographic characteristics distinguish Fortune Bay from other fjordic systems: it is 'semi-opened' to the coastal ocean, being surrounded by long sills (<100 m mean depth) and subject to renewal from two basins (reservoir) of very distinct water masses which greatly affect its renewal dynamics (e.g. limited to no need for 'preconditioning').

We investigated the seasonal cycle of its physical water structure (temperature and salinity) and of the forces acting upon it (freshwater input, tide and wind). These forces, in turn drive the motion of its waters. Special attention is given to the upper layers (above sill levels) circulation, by extracting and quantifying the main components (mean seasonal circulation, weather band, tidal band and high-frequency band) and describing what appear to be the dominant dynamics (qualified herein as 'pulses'). Previous studies on bottom water renewal are summarized and slightly extended using water profiles collected more recently. Estimates of water exchanges from the main processes identified and corresponding flushing times of the inner part of the bay, where the aquaculture activities occur, are also provided to get a quantitative sense of their importance. Limited attention was given to the long-term and interannual variability, largely due to lack of data to do it but also because the focus of this study was on what is likely to be the dominant cycle (seasonal) and modes of variability (weather band). Yet, an estimate of recent sea-surface warming is provided which is both important in comparison with the global rate (factor 4) and characterized by a strong seasonality (factor 2 between the largest rate in summer and the lowest rate in winter).

From this study, it appears that wind forcing and baroclinic pumping, to which the wind certainly plays a role, are the dominant sources of currents variability and thus, possibly of water exchange within the fjord itself but also between the fjord and the shelf. Very similar processes have been reported in other

large embayments of Newfoundland which suggest their potentially ubiquitous nature in the region. While we hope to fill an important knowledge gap of this interesting and economically important area, much remains to be elucidated. Most importantly, perhaps, will be to clearly identify the nature and origin of the current 'pulses', described herein, i.e. the physical process and the forcing responsible for their generation. The role of the wind as the main forcing mechanism and the ocean response time to this forcing need to be assessed more definitely, for instance, and this will be the focus of further studies. Given their importance to the ecosystem and aquaculture as well as fisheries activities occurring in this region, dedicated studies based on more elaborate methods such as box modelling or fully three dimensional modelling will also be needed to refine the first estimates of flushing provided herein.

Declaration of competing interest

Data availability

Data are publicly available from https://doi.org/10.6084/m9. figshare.13526366 and https://doi.org/10.17882/62314.

Acknowledgments

Funding

Appendix A. Supplementary data

Supplementary material related to this article can be found online at https://doi.org/10.1016/j.rsma.2022.102698.

References

Aure, J., Molvær, J., Stigebrandt, A., 1996. Observations of inshore water exchange forced by a fluctuating offshore density field. Mar. Pollut. Bull. 33, 112–119. http://dx.doi.org/10.1016/S0025-326X(97)00005-2.

Belkin, I.M., 2009. Rapid warming of large marine ecosystems. Prog. Oceanogr. 81, 207–213. http://dx.doi.org/10.1016/j.pocean.2009.04.011.

Bezaud, M., Lazure, P., Le Cann, B., 2020. Wind-induced barotropic oscillations around the Saint Pierre and Miquelon archipelago (North-West Atlantic). Cont. Shelf Res. 195, 104062. http://dx.doi.org/10.1016/j.csr.2020.104062.

Bisagni, J.J., Seemann, K.W., Mavor, T.P., 2001. High-resolution satellite-derived sea-surface temperature variability over the Gulf of Maine and Georges Bank region, 1993–1996. Deep Sea. Res. II: Top. Stud. Oceanogr. 48, 71–94. http://dx.doi.org/10.1016/S0967-0645(00)00115-6.

Blais, M., Galbraith, P.S., Plourde, S., Devred, E., Clay, S., Lehoux, C., Devine, L., 2021. Chemical and Biological Oceanographic Conditions in the Estuary and Gulf of St. Lawrence during 2020 (DFO Can. Sci. Advis. Sec. Res. Doc. No. 2021/060). https://waves-vagues.dfo-mpo.gc.ca/library-bibliotheque/41012008.pdf (accessed 26-Sep-2022).

Burchard, H., Bolding, K., Feistel, R., Gräwe, U., Klingbeil, K., MacCready, P., Mohrholz, V., Umlauf, L., van der Lee, E.M., 2018. The Knudsen theorem and the Total Exchange Flow analysis framework applied to the Baltic Sea. Prog. Oceanogr. 165, 268–286. http://dx.doi.org/10.1016/j.pocean.2018.04.004.

Canadian Hydrographic Survey (CHS), 2021. Canadian Sailing Directions, General Information, Atlantic Coast (No. 12/2021). Fisheries and Oceans Canada. https://waves-vagues.dfo-mpo.gc.ca/Library/chs-shc-ATL100-eng-202112-4105457x.pdf (accessed 26-Sep-2022).

Canadian Ice Services (CIC), 2011. Sea Ice Climatic Atlas. East Coast 1981-2010. Environment Canada, https://publications.gc.ca/collections/collection_2013/ec/En57-38-2010-eng.pdf (accessed 26-Sep-2022).

Casey, K.S., Brandon, T.B., Cornillon, P., Evans, R., 2010. The past, present, and future of the AVHRR pathfinder SST program. In: Barale, V., Gower, J.F.R., Alberotanza, L. (Eds.), Oceanography from Space. Springer Netherlands, Dordrecht, pp. 273–287. http://dx.doi.org/10.1007/978-90-481-8681-5_16.

Cottier, F.R., Nilsen, F., Skogseth, R., Tverberg, V., Skarðhamar, J., Svendsen, H., 2010. Arctic fjords: a review of the oceanographic environment and dominant physical processes. SP 344, 35–50. http://dx.doi.org/10.1144/SP344.4.

Courtier, A., 1939. Classification of tides in four types. In: The International Hydrographic Review.

Cyr, F., Larouche, P., 2015. Thermal fronts atlas of Canadian coastal waters. Atmos.-Ocean 53, 212–236. http://dx.doi.org/10.1080/07055900.2014.986710.

Cyr, F., Snook, S., Bishop, C., Galbraith, P.S., Chen, N., Han, G., 2022. Physical Oceanographic Conditions on the Newfoundland and Labrador Shelf During 2021 (DFO Can. Sci. Advis. Sec. Res. Doc. No. 2022/040). https://waves-vagues.dfo-mpo.gc.ca/library-bibliotheque/40960754.pdf (accessed 26-Sep-2022).

Davidson, F.J.M., Greatbatch, R.J., de Young, B., 2001. Asymmetry in the response of a stratified coastal embayment to wind forcing. J. Geophys. Res. 106, 7001–7015. http://dx.doi.org/10.1029/2000JC900052.

de Young, B., 1983. Deep water exchange in Fortune Bay, Newfoundland (M.Sc. thesis). Memorial University of Newfoundland, St. John's, NL, http://research.library.mun.ca/id/eprint/5754 (accessed 26-Sep-2022).

de Young, B., Hay, A.E., 1987. Density current flow into Fortune Bay, Newfoundland. J. Phys. Oceanogr. 17, 1066–1070. http://dx.doi.org/10.1175/1520-0485(1987)017<1066:DCFIFB>2.0.CO;2.

de Young, B., Otterson, T., Greatbatch, R.J., 1993. The local and nonlocal response of conception bay to wind forcing. J. Phys. Oceanogr. 23, 2636–2649.

DFO, 2016. State of Knowledge of the Oceanography and Water Exchange on the South Coast of Newfoundland to Support the Development of Bay Management Areas for Finfish Aquaculture (DFO Can. Sci. Advis. Sec. Sci. Advis. Rep. No. 2016/039). Fisheries and Oceans Canada, https://waves-vagues.dfo-mpo.gc.ca/library-bibliotheque/40595134.pdf (accessed 26-Sep-2022).

Donnet, S., Cross, S., Goulet, P., Ratsimandresy, A.W., 2018a. Coast of Bays Seawater Vertical and Horizontal Structure (2009-13): Hydrographic Structure, Spatial Variability and Seasonality Based on the Program for Aquaculture Regulatory Research (PARR) 2009-13 oceanographic surveys (DFO Can. Sci. Advis. Sec. Res. Doc. No. 2017/077). https://waves-vagues.dfo-mpo.gc.ca/library-bibliotheque/40655945.pdf (accessed 26-Sep-2022).

Donnet, S., Lazure, P., Ratsimandresy, A., Han, G., 2020. A comprehensive oceanographic dataset of a subpolar, mid-latitude broad fjord: Fortune Bay, Newfoundland, Canada. Earth Syst. Sci. Data 12, 1877–1896. http://dx.doi.org/10.5194/essd-12-1877-2020.

Donnet, S., Ratsimandresy, A.W., Goulet, P., Doody, C., Burke, S., Cross, S., 2018b. Coast of Bays Metrics: Geography, Hydrology and Physical Oceanography of an Aquaculture Area of the South Coast of Newfoundland (DFO Can. Sci. Advis. Sec. Res. Doc. No. 2017/076). https://waves-vagues.dfo-mpo.gc.ca/library-bibliotheque/40654473.pdf (accessed 26-Sep-2022).

Fader, G.B., King, L.H., Josenhans, H.W., 1982. Surficial geology of the Laurentian Channel and the western Grand Banks of Newfoundland. Fisheries and Oceans, Scientific Information and Publication, Ottawa, Canada.

Farmer, D.M., Freeland, H.J., 1983. The physical oceanography of fjords. Prog. Oceanogr. 12, 147–219. http://dx.doi.org/10.1016/0079-6611(83)90004-6.

Galbraith, P.S., Chassé, J., Shaw, J.L., Dumas, J., Caverhill, C., Lefaivre, D., Lafleur, C., 2021. Physical Oceanographic Conditions in the Gulf of St. Lawrence during 2020 (DFO Can. Sci. Advis. Sec. Res. Doc. No. 2021/045). https://waves-vagues.dfo-mpo.gc.ca/library-bibliotheque/40980856.pdf (accessed 26-Sep-2022).

Galbraith, P.S., Larouche, P., 2013. Trends and variability in eastern canada sea-surface temperatures. In: Aspects of Climate Change in the Northwest Atlantic off Canada, Can. Tech. Rep. Fish. Aquat. Sci. pp. 1–18, https://waves-vagues.dfo-mpo.gc.ca/Library/350208.pdf (accessed 26-Sep-2022).

Garrett, C., Munk, W., 1972. Space-time scales of internal waves. Geophys. Fluid Dyn. 3, 225–264. http://dx.doi.org/10.1080/03091927208236082.

Garrett, C., Munk, W., 1975. Space–time scales of internal waves: A progress report. J. Geophys. Res. 80, 291–297. http://dx.doi.org/10.1029/JC080i003p00291.

Gillibrand, P.A., 2001. Calculating exchange times in a scottish fjord using a two-dimensional, laterally-integrated numerical model. estuarine. Coast. Shelf Sci. 53, 437–449. http://dx.doi.org/10.1006/ecss.1999.0624.

Gillpatrick, W.W., Gibson, John, 1884. Newfoundland and Labrador: The Coast and Banks of Newfoundland, and the Coast of Labrador, from Grand Point to the Koksoak River, with the Adjacent Islands and Banks, U.S. Hydrographic Office. Government Printing Office, Washington.

Gregory, D.N., 2004. Climate : Une base de données d'observations de la température et de la salinité pour le nord-ouest de l'Atlantique (DFO Can. Sci. Advis. Sec. Res. Doc. No. 2004/075). Fisheries and Oceans Canada, https://waves-vagues.dfo-mpo.gc.ca/library-bibliotheque/284130.pdf (accessed 26-Sep-2022).

Grinsted, A., Moore, J.C., Jevrejeva, S., 2004. Application of the cross wavelet transform and wavelet coherence to geophysical time series. Nonlin. Processes. Geophys. 11, 561–566. http://dx.doi.org/10.5194/npg-11-561-2004.

Han, G., 2005. Wind-driven barotropic circulation off Newfoundland and Labrador. Cont. Shelf Res. 25, 2084–2106. http://dx.doi.org/10.1016/j.csr.2005.04.015.

Han, G., Lu, Z., Wang, Z., Helbig, J., Chen, N., de Young, B., 2008. Seasonal variability of the Labrador Current and shelf circulation off Newfoundland. J. Geophys. Res. 113, C10013. http://dx.doi.org/10.1029/2007JC004376.

Han, G., Ma, Z., Chen, D., deYoung, B., Chen, N., 2012. Observing storm surges from space: Hurricane Igor off Newfoundland. Sci. Rep. 2, 1010. http://dx.doi.org/10.1038/srep01010.

Han, G., Ma, Z., deYoung, B., Foreman, M., Chen, N., 2011. Simulation of three-dimensional circulation and hydrography over the Grand Banks of Newfoundland. Ocean Model. 40, 199–210. http://dx.doi.org/10.1016/j.ocemod.2011.08.009.

Hargrave, B.T., Silvert, W., Keizer, P.D., 2005. Assessing and managing environmental risks associated with marine finfish aquaculture. In: Hargrave, B.T. (Ed.), Environmental Effects of Marine Finfish Aquaculture. In: Handbook of Environmental Chemistry, Springer-Verlag, Berlin/Heidelberg, pp. 433–461. http://dx.doi.org/10.1007/b136021.

Hay, A.E., de Young, B., 1989. An oceanographic flip-flop: deep water exchange in Fortune Bay. Newfoundland. J. Geophys. Res. 94, 843. http://dx.doi.org/10.1029/JC094iC01p00843.

Inall, M.E., Gillibrand, .P.A., 2010. The physics of mid-latitude fjords: a review. SP 344, 17–33. http://dx.doi.org/10.1144/SP344.3.

Inall, M.E., Nilsen, F., Cottier, F.R., Daae, R., 2015. Shelf/fjord exchange driven by coastal-trapped waves in the A rctic. J. Geophys. Res. Oceans 120, 8283–8303. http://dx.doi.org/10.1002/2015JC011277.

IOC, SCOR, IAPSO, 2010. The International Thermodynamic Equation of Seawater – 2010: Calculation and Use of Thermodynamic Properties (Manuals and Guides No. 56). UNESCO.

IPCC, 2014. Climate Change 2014: Synthesis Report. Contribution of Working Groups I, II and III to the Fifth Assessment Report of the Intergovernmental Panel on Climate Change. IPCC, Geneva, Switzerland, https://www.ipcc.ch/site/assets/uploads/2018/02/SYR_AR5_FINAL_full.pdf (accessed 26-Sep-2022).

Large, W.G., Pond, S., 1981. Open ocean momentum flux measurements in moderate to strong winds. J. Phys. Oceanogr. 11, 324–336. http://dx.doi.org/10.1175/1520-0485(1981)011<0324:OOMFMI>2.0.CO;2.

Lauzier, L.M., Trites, R.W., 1958. The deep waters in the laurentian channel. J. Fish. Res. Bd. Can 15, 1247–1257. http://dx.doi.org/10.1139/f58-068.

Levine, M.D., Paulson, C.A., Briscoe, M.G., Weller, R.A., Peters, H., 1983. Internal waves in JASIN. Philos. Trans. R. Soc. Lond. A Math. Phys. Eng. Sci. 308, 389–405. http://dx.doi.org/10.1098/rsta.1983.0011.

Loder, J.W., Petrie, B., Gawarkiewicz, G., 1998. The coastal ocean off northeastern North America: A large-scale view. The sea 11, 105–138.

Ma, Z., Han, G., Chassé, J., 2016. Simulation of circulation and ice over the Newfoundland and Labrador Shelves: the mean and seasonal cycle. Atmos.-Ocean 54, 248–263. http://dx.doi.org/10.1080/07055900.2015.1077325.

Ma, Z., Han, G., deYoung, B., 2012. Modelling temperature, currents and stratification in Placentia Bay. Atmos.-Ocean 50, 244–260. http://dx.doi.org/10.1080/07055900.2012.677413.

Ma, Z., Han, G., Young, B., 2015. Oceanic responses to H urricane I gor over the G rand B anks: A modeling study. J. Geophys. Res. Oceans 120, 1276–1295. http://dx.doi.org/10.1002/2014JC010322.

MacCready, P., Geyer, W.R., Burchard, H., 2018. Estuarine exchange flow is related to mixing through the salinity variance budget. J. Phys. Oceanogr. 48, 1375–1384. http://dx.doi.org/10.1175/JPO-D-17-0266.1.

McDougall, T.J., Barker, M., 2011. Getting started with TEOS-10 and the Gibbs Seawater (GSW) Oceanographic Toolbox (No. ISBN 978-0-646-55621-5). SCOR/IAPSO WG127.

McLellan, H.J., 1957. On the distinctness and origin of the slope water off the scotian shelf and its easterly flow south of the Grand Banks. J. Fish. Res. Bd. Can. 14, 213–239. http://dx.doi.org/10.1139/f57-011.

Myers, R.A., Akenhead, S.A., Drinkwater, K., 1990. The influence of Hudson Bay runoff and ice-melt on the salinity of the inner Newfoundland Shelf. Atmos.-Ocean 28, 241–256. http://dx.doi.org/10.1080/07055900.1990.9649377.

Pawlowicz, R., 2013. What Every Oceanographer Needs to Know about TEOS-10 (The TEOS-10 Primer); v8 (April 2013). UNESCO-IOS Unpublished manuscript. Available at www.TEOS-10.org.

Pawlowicz, R., Beardsley, B., Lentz, S., 2002. Classical tidal harmonic analysis including error estimates in MATLAB using T_TIDE. Comput. Geosci. 28, 929–937. http://dx.doi.org/10.1016/S0098-3004(02)00013-4.

Petrie, B., Anderson, C., 1983. Circulation on the newfoundland continental shelf. Atmos.-Ocean 21, 207–226. http://dx.doi.org/10.1080/07055900.1983.9649165.

Pisano, A., Marullo, S., Artale, V., Falcini, F., Yang, C., Leonelli, F.E., Santoleri, R., Buongiorno Nardelli, B., 2020. New evidence of mediterranean climate change and variability from sea surface temperature observations. Remote Sens. 12, 132. http://dx.doi.org/10.3390/rs12010132.

Plante, M., Son, S.-W., Atallah, E., Gyakum, J., Grise, K., 2015. Extratropical cyclone climatology across eastern canada. Int. J. Climatol. 35, 2759–2776. http://dx.doi.org/10.1002/joc.4170.

Poitevin, P., Lazure, P., Roy, V., Donnet, S., Chauvaud, L., 2022. The 18.6-year lunar nodal cycle may affect ecosystems on the Northwest Atlantic continental shelves. J. Mar. Syst. 235, 103783. http://dx.doi.org/10.1016/j.jmarsys.2022.103783.

Ratsimandresy, A.W., Donnet, S., Goulet, P., 2020. Identification of geographic zones of influence associated with surface circulation for Aquaculture Bay Management Area application. J. Mar. Syst. 204, 103291. http://dx.doi.org/10.1016/j.jmarsys.2019.103291.

Ratsimandresy, A.W., Donnet, S., Goulet, P., Bachmayer, R., Claus, B., 2014. Variation in the structure of the water column as captured by Slocum glider CTD and by CTD from a research vessel and assessment of internal waves. In: 2014 Oceans - St. John's. Presented at the OCEANS 2014. IEEE, St. John's, NL, pp. 1–10. http://dx.doi.org/10.1109/OCEANS.2014.7003283.

Ratsimandresy, A.W., Donnet, S., Snook, S., Goulet, P., 2019. Analysis of the variability of the ocean currents in the Coast of Bays area (DFO Can. Sci. Advis. Sec. Res. Doc. No. 2019/008). https://waves-vagues.dfo-mpo.gc.ca/library-bibliotheque/40805116.pdf (accessed 26-Sep-2022).

Richard, J.M., 1987. The Mesopelagic Fish and Invertebrate Macrozooplankton Faunas of Two Newfoundland Fjords with Differing Physical Oceanography (M.Sc. thesis). Memorial University of Newfoundland, http://research.library.mun.ca/id/eprint/4196 (accessed 26-Sep-2022).

Richard, J.M., Haedrich, R.L., 1991. A comparison of the macrozooplankton faunas in two newfoundland fjords differing in physical oceanography. Sarsia 76, 41–52. http://dx.doi.org/10.1080/00364827.1991.10413465.

Saha, K., Zhao, X., Zhang, H.-M., Casey, K.S., Zhang, D., Baker-Yeboah, S., Kilpatrick, K.A., Evans, R.H., Ryan, T., Relph, J.M., 2018. AVHRR Pathfinder version 5.3 level 3 collated (L3C) global 4km sea surface temperature for 1981-Present. X. http://dx.doi.org/10.7289/V52J68X.

Salcedo-Castro, J., Ratsimandresy, A.W., 2013. Oceanographic response to the passage of hurricanes in Belle Bay, Newfoundland. Estuar. Coast. Shelf Sci. 133, 224–234. http://dx.doi.org/10.1016/j.ecss.2013.08.031.

Stigebrandt, A., 2012. Hydrodynamics and circulation of fjords. Encycl. Lakes Reserv. 327, 344.

Tang, C.L., Gui, Q., DeTracey, B.M., 1998. Barotropic response of the labrador/newfoundland shelf to a moving storm. J. Phys. Oceanogr. 28, 1152–1172. http://dx.doi.org/10.1175/1520-0485(1998)028<1152:BROTLN>2.0.CO;2.

Thiebaut, S., Vennell, R., 2010. Observation of a fast continental shelf wave generated by a storm impacting newfoundland using wavelet and cross-wavelet analyses. J. Phys. Oceanogr. 40, 417–428. http://dx.doi.org/10.1175/2009JPO4204.1.

Verbrugge, N., Reverdin, G., 2003. Contribution of horizontal advection to the interannual variability of sea surface temperature in the North Atlantic. J. Phys. Oceanogr. 33, 964–978. http://dx.doi.org/10.1175/1520-0485(2003)033<0964:COHATT>2.0.CO;2.

Wang, Z., Yashayaev, I., Greenan, B., 2015. Seasonality of the inshore Labrador current over the Newfoundland shelf. Cont. Shelf Res. 100, 1–10. http://dx.doi.org/10.1016/j.csr.2015.03.010.

White, M., Hay, A.E., 1994. Dense overflow into a large silled embayment: Tidal modulation, fronts and basin modes. 52, (ISSN: 0022-2402) pp. 459–487. http://dx.doi.org/10.1357/0022240943077055.

Yao, T., 1986. The response of currents in Trinity Bay, Newfoundland, to local wind forcing. Atmosphere-Ocean 24, 235–252. http://dx.doi.org/10.1080/07055900.1986.9649249.